Geochemical and Nd-Sr Isotopic Compositions of Hypabyssal Adakites in the Torud-Ahmad Abad Magmatic Belt, Northern Central Iran Zone: Analysis of Petrogenesis and Geodynamic Implications

Fazilat Yousefi ⓘD*[1], **Ryan D. Mills**[2], **Mahmoud Sadeghian**[3], **David R. Lentz** ⓘD[1], **Christina Wanhainen**[4], **Habibollah Ghasemi**[3], **Laicheng Miao**[5]

1. *Department of Earth Sciences, University of New Brunswick, Fredericton, Canada*
2. *Department of Geological Sciences, University of North Carolina at Chapel Hill, Chapel Hill, USA*
3. *Faculty of Earth Sciences, Shahrood University of Technology, Shahrood, Iran*
4. *Department of Civil, Environmental and Natural Resources Engineering, Lulea University of Technology, Lulea, Sweden*
5. *Institute of Geology and Geophysics, Chinese Academy of Sciences, Beijing 100029, China*

ⓘD Fazilat Yousefi: https://orcid.org/0000-0001-6081-790X; ⓘD David R. Lentz: https://orcid.org/0000-0002-9562-6211

ABSTRACT: Eocene intermediate to felsic subvolcanic rocks of the Torud-Ahmad Abad magmatic belt (TAMB), in the northern part of the Central Iran zone, are exposed between the Torud and Ahmad Abad regions in South-Southeast Shahrood. These igneous rocks include hypabyssal dacite, trachyte, andesite, trachy-andesite, and basaltic andesite; they are mainly composed of phenocrysts and microcrystalline groundmass of pyroxene, amphibole, and plagioclase, with minor biotite and titanomagnetite; they form domal structures (plugs and stocks), dikes, and sills that intruded into Neoproterozoic to cogenetic Eocene volcano-sedimentary sequences. Based on isotopic analysis of these intermediate to acidic rocks, initial ratios of $^{143}Nd/^{144}Nd$ range from 0.512 775 to 0.512 893 and initial ratios of $^{87}Sr/^{86}Sr$ range from 0.703 746 to 0.705 314, with quite positive $\varepsilon_{Nd(i)}$ values of +3.69 to +6.00. They are enriched in light rare earth elements and large ion lithophile elements and depleted in heavy rare earth elements and high-field strength elements, the SiO_2 content is (52–62) wt.%, and Na_2O content >3 wt.%, Al_2O_3 content >16 wt.%, Yb <1.8 ppm, and Y <18 ppm. These geological, geochemical, and Sr and Nd isotopic data are consistent with adakitic signatures originating by partial melting of the subducted Neo-Tethys oceanic slab (Sabzevar branch) and lithospheric suprasubduction zone mantle. The mantle signatures typifying the rapidly emplaced adakitic rocks (slab (high-silica adakite) and suprasubduction zone (low-silica adakite) melts) together with their locally voluminous extent are evidences that support a locally extensional geodynamic setting; and the evidence is consistent with an evolution to local transpression in the Late Eocene in this convergent margin arc environment to rifting (basalts to adakites) towards submarine conditions in the Neogene.

KEY WORDS: isotope geochemistry, adakite rocks, Central Iran zone, Shahrood, Iran.

0 INTRODUCTION

Iran is an ideal region for studying collisional processes and Iranian Plateau development due to the relatively recent nature of the Arabia-Eurasia collision (e.g., Guest et al., 2007). The geology and tectonics of Iran are highly influenced by the evolution of the Tethyan oceans (Mehdipour Ghazi and Moazzen, 2015).
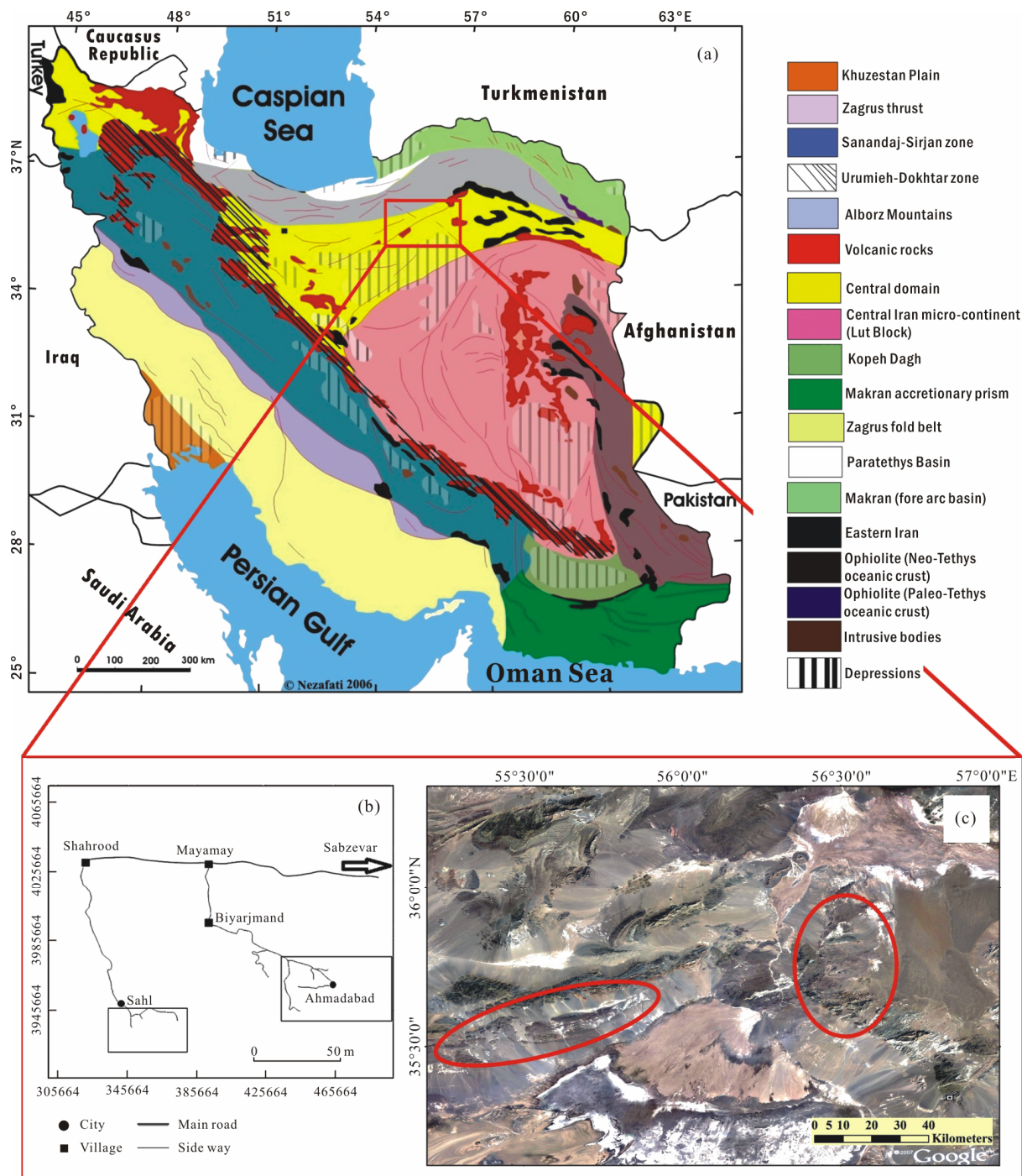
The northern part of the Central Iran zone includes several magmatic belts, e.g., Davarzan-Abbasabad Eocene volcanic magmatic belt in the northern part of the Sabzevar City investi-

gated by Ghasemi and Rezaei-Kahkhaei (2015) and the Torud-Ahmad Abad magmatic belt (TAMB), South-Southeast Shahrood (Fig. 1), presented by Yousefi et al. (2017a). The Davarzan-Abbasabad Eocene magmatic belt consists of arc-like Paleocene to Eocene magmatism and post-subduction Oligocene to Quaternary magmatism (Ghasemi and Rezaei-Kahkhaei, 2015). The TAMB consists of intermediate to felsic subvolcanic domes and dikes that cut Eocene volcano-sedimentary rocks (Yousefi et al., 2017a, b) (Fig. 1). As shown in Table 1, basaltic andesite rocks differ in the amount of silica from other rocks, but they have been studied alongside because they have penetrated older units and are similar to others in some geochemical properties. Geochemical examinations of the TAMB volcanic rocks revealed that they consist of andesite, trachyandesite, dacite, trachyte, and basaltic andesite with many mafic clots and mafic microgranular enclaves (MME). The existence of enclaves with different compositions

Figure 1. Sketch map showing the distribution of the Middle and Late Eocene subvolcanic rocks of the Torud-Ahmad Abad magmatic belt (TAMB) in the northern part of Central Iran structural zone (map redrawn from Nezafati, 2015). The red rectangle on the map of Iran shows the Torud-Ahmad Abad magmatic belt. The horizontal ellipse on the satellite image is the Torud region and the vertical ellipse is the Ahmad Abad region.

suggests a rapid emplacement process into the upper crust (Yousefi et al., 2017b). These enclaves are cogenetic and non-cogenetic in origin. The types and characteristics of these enclaves are discussed in detail in Yousefi et al. (2017a, b). Mafic enclaves dominantly consist of just pyroxene and hornblende. Another group of the enclaves is xenoliths that originated from the lithospheric mantle, which were entrained during rapid ascent (Yousefi et al., 2017a). The crustal xenoliths include gneiss, amphibolite, carbonate-bearing tuff (30 to 50 cm), tonalite, and leucogabbro xenoliths.

Yousefi et al. (2017a) also noted that the depletion of Nb and Ti, and enrichment in Rb, Ba, K, and Th imply crustal contamination (and/or subduction erosion to assimilation during ascent) of these adakitic magmas, which includes andesitic and dacitic rocks in the TAMB. Based on lithogeochemical analyses (Table 1), the igneous rocks in TAMB are classified as adakite or adakite-like. The U-Pb zircon geochronology (Yousefi et al., 2017a) obtained ages of 41.4±0.3 Ma (andesite) and 35.5±0.2 Ma (dacite) from two TAMB samples. The Middle to Late Eocene TAMB subvolcanic rocks have intruded into the host

sedimentary and volcanic units (Fig. 2). These Eocene subvolcanic rocks are covered by younger sequences consisting of intercalations of submarine rift basalts, locally with adakitic dikes, marl, red beds of Oligo–Miocene, and Neogene sandstones to conglomerates. Finally, the entire sequence is partially covered by stream sediments and alluvial fan sediments. In this paper, major and trace element geochemical information and Sr and Nd isotopic determinations on the subvolcanic rocks of Torud-Ahmad Abad magmatic belt help to clarify their petrogenesis. In addition to what is presented in this article, we have tried to discuss the relationship between these adakites and the TTGs units of Archean age.

1 GEOLOGICAL BACKGROUND

The TAMB is located ~150 km south-southeast of Shahrood in the northern part of the Central Iran zone (Fig. 1), which is divided into two major parts in the south and southeast of Shahrood (between the two villages in the Torud-Ahmad Abad region). The basement is divided into four general groups (Hosseini et al., 2015; Balaghi Einalou et al., 2014): (1) metapelitic rocks include phyllite, mica schists, garnet-bearing schists, and gneisses; (2) metasandstones include metapsammites and metagraywackes; (3) metabasites include amphibolitic schists, amphibolites, and garnet amphibolites with an igneous protolith; (4) metacarbonates include calcite or dolomite marbles in the upper parts of this sequence (Fig. 2). The ages of the Neoproterozoic gneisses obtained by U-Pb zircon dating are 546.0±0.7 to 547.0±6.8 Ma (Yousefi, 2017; Balaghi Einalou et al., 2014).

The Central Iran zone was tectonically active during the Mesozoic and Cenozoic (Yousefi et al., 2017a) and, according to this, igneous activity developed in the forms of volcanic, subvolcanic, and intrusive rocks. Most of the magmas in this part
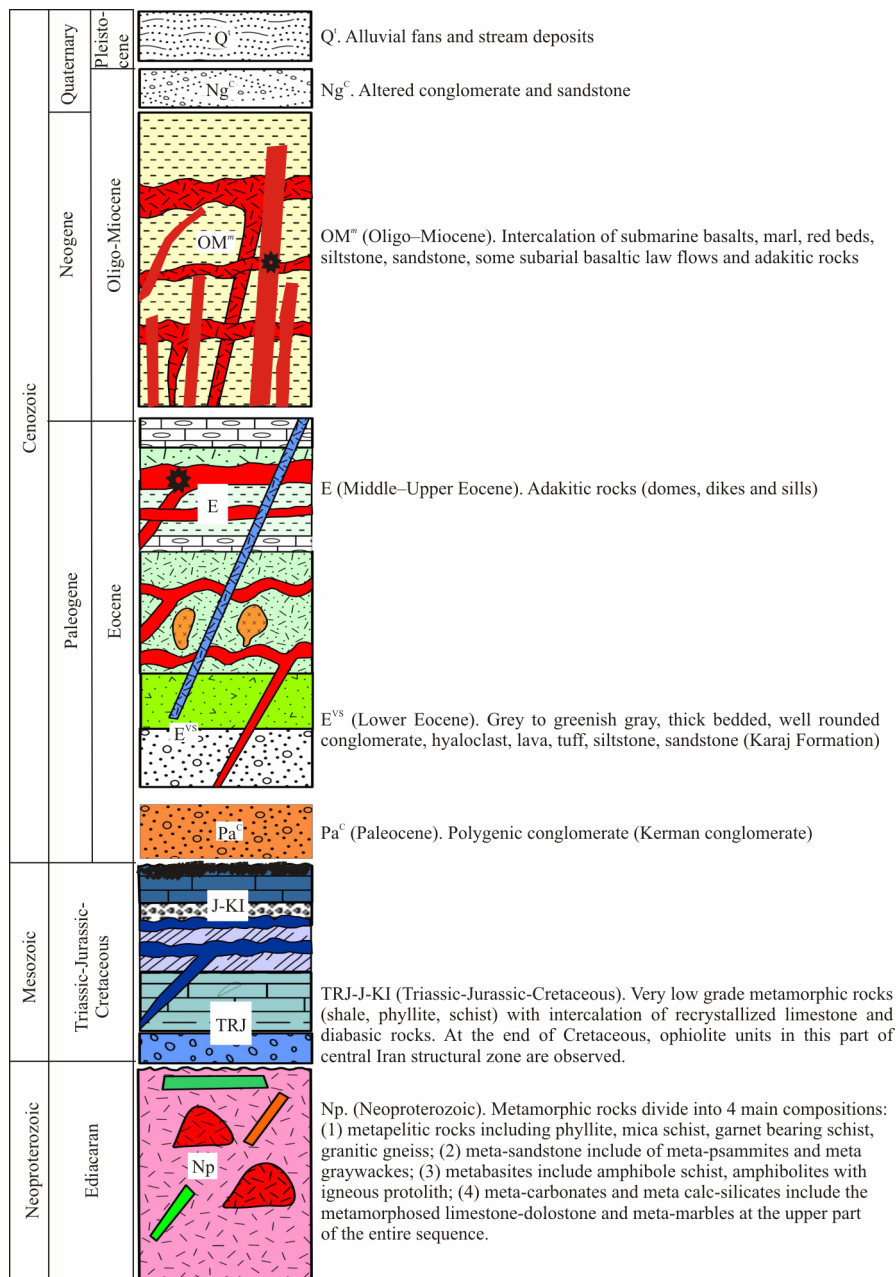
Figure 2. Stratigraphic section of the TAMB. The age range of these units are between Neoproterozoic to Eocene.
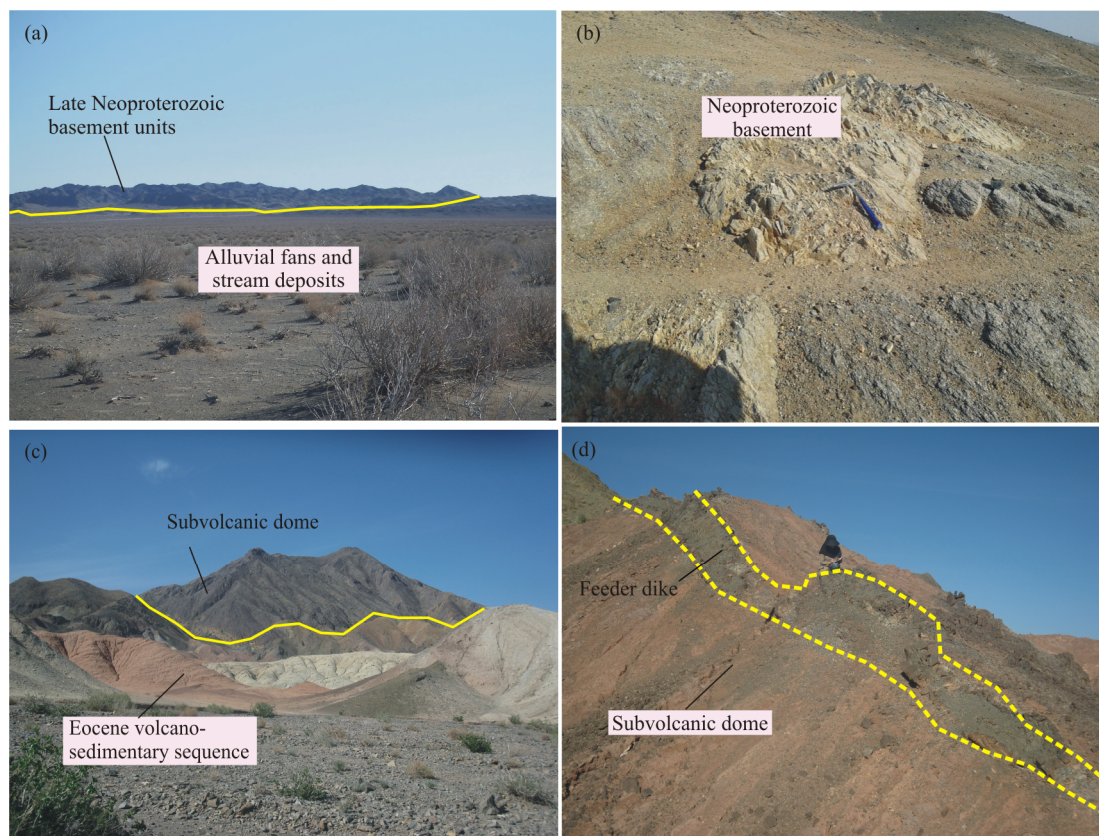
Figure 3. Field photographs showing (a) and (b) Late Neoproterozoic basement units; (c) Bazmin, one of the subvolcanic domes, which intruded in the Eocene volcano-sedimentary sequence; (d) basaltic andesite feeder dikes fed the subvolcanic domes south-southeast of Shahrood.

of the Central Iran zone are Cenozoic in age (Yousefi et al., 2017a, b). In the north of the Central Iran zone, the extensive Mesozoic and Cenozoic volcanic and subvolcanic rocks cover much older rock units (Fig. 3c). In some places, the subvolcanic adakitic domes in the TAMB were fed by dikes visible in the region.

2 ANALYTICAL METHODS

Three hundred samples from the TAMB were collected during mapping work. After detailed petrographic studies, 12 representative samples were selected for lithogeochemical analysis (Table 1). These 12 samples were analyzed by inductively coupled plasma-optical emission spectroscopy (ICP-OES) after fusion of 0.20 g of rock powder with 1.50 g $LiBO_2$ and dissolved in 100 mL 5% HNO_3. Trace elements were determined using inductively coupled plasma-mass spectrometry (ICP-MS) at ALS Chemex in Canada. The detection limits for ICP-OES and ICP-MS range of 0.01 wt.%–0.10 wt.% for major oxides, 0.1 ppm–10 ppm for trace elements, and 0.01 ppm–0.5 ppm for REEs. Loss on ignition (LOI) was determined by drying the samples heated at 1 050 °C. The extensive new Sr and Nd isotopic compositions were determined for 14 whole-rock samples at Geochronology and Isotope Geochemistry Laboratory, University of North Carolina, Chapel Hill, USA (samples FY-2-2, FR-6, FY-7, FR-26, FR-32) and Institute of Geology and Geophysics, Chinese Academy of Sciences, Beijing, China (samples FY-33, FY-35, FR-63, FR-28, FR-20).

Whole-rock powder was dissolved using HF and HNO_3 in Teflon bombs at approximately 180 °C for >48 to 72 hours. Sam-

ples were then dried and fluxed in concentrated HCl for 8 to 16 hours. Aliquoted samples for isotope determination was done based on estimated or previously determined concentrations. Strontium was purified using Sr exchange resin (see Lundblad, 1994) and loaded on single Re filaments with a TaF_5 activator to enhance ionization. Neodymium was purified in a three-stage column procedure (see Harvey and Baxter, 2009). Total procedural blanks were less than 0.1 ng for Sr and 0.02 ng for Nd. Whole-rock Sr and Nd isotopes were determined on the Isotopic PhoenixX62 TIMS at the University of North Carolina (Chapel Hill). Strontium was analyzed as a metal in dynamic multicollector mode with $^{88}Sr=3V$. Strontium isotope ratios are corrected for mass fractionation using an exponential law correction and normalized to $^{86}Sr/^{88}Sr=0.119\ 4$. Replicate analyses of the NBS 987 Sr standard yielded $^{87}Sr/^{86}Sr=0.710\ 243\pm0.000\ 011$ (2σ, n=10). Neodymium was determined in dynamic-multicollector mode with $^{147}Sm=3V$, $^{142}Nd^{16}O=1V$. Neodymium isotope compositions were normalized to $^{146}Nd/^{144}Nd=0.721\ 9$ and referenced to $^{143}Nd/^{144}Nd=0.512\ 115\pm0.000\ 012$ (JNdi, n=20). Epsilon notation was calculated using the present day CHUR value of $^{143}Nd/^{144}Nd=0.512\ 638$. Epsilon values for Nd at crystallization age (t) using $^{143}Nd/^{144}Nd$ (CHUR, 0 Ma)=0.512 638 and $^{147}Sm/^{144}Nd$ (CHUR, 0 Ma)=0.196 7.

Whole-rock powders for Sr and Nd isotopic determinations were dissolved in Savillex Teflon screw-top capsule after spiking with a mixed ^{87}Rb-^{84}Sr and ^{149}Sm-^{150}Nd tracers prior to HF+HNO_3+$HClO_4$ acid dissolution. Rubidium, Sr, Sm, and Nd were separated using an accepted two-step ion exchange

Table 1 Whole-rock major elements (wt.%), trace elements and REEs (ppm) of Eocene volcanic and intrusive rocks of the Torud-Ahmadabad magmatic belt (northern part of CISZ), south-southeast of Shahrood

Sample No.	FY-2-2	FY-35	FR-63	FR-28	FR-20	FR-6	FR-11	FY-7	FY-33	FR-26	MF-21	FR-32
SiO_2	59.8	61.4	56.8	54.4	55.9	45.5	52.6	61.6	62.0	53.6	49.3	45.0
Al_2O_3	18.70	19.05	17.50	18.75	17.30	18.30	20.50	17.10	18.55	18.10	17.42	17.30
$Fe_2O_3^T$	4.38	4.55	6.83	7.03	7.04	9.81	6.20	4.82	4.59	7.29	9.83	10.95
MgO	1.66	2.02	3.21	3.60	3.79	5.18	2.44	2.74	2.33	4.22	3.71	8.09
CaO	4.88	5.78	5.86	7.30	6.33	7.84	3.64	5.09	5.46	6.87	13.68	10.65
Na_2O	4.38	3.78	3.65	4.22	3.88	5.00	6.05	4.92	4.00	5.30	2.34	3.05
K_2O	1.18	0.92	2.62	2.06	2.62	1.66	2.90	1.17	1.03	2.59	1.91	2.07
TiO_2	0.48	0.53	0.37	0.53	0.49	0.73	0.63	0.55	0.53	0.58	0.69	0.89
P_2O_5	0.22	0.28	0.20	0.21	0.15	0.36	0.40	0.22	0.26	0.23	0.23	0.24
MnO	0.09	0.10	0.12	0.12	0.15	0.22	0.15	0.08	0.08	0.14	0.13	0.16
LOI	2.46	2.52	2.76	1.25	2.19	3.27	2.82	2.99	2.36	2.56	2.75	2.33
Total	98.4	101.0	100.1	99.6	100.0	98.0	98.5	101.4	101.3	101.6	100.6	100.9
Sc	5	8	14	16	16	23	10	7	8	18	29	38
Ba	374	225	415	264	320	477	531	265	222	226	120.5	290
Cs	0.42	0.25	1.81	2.05	1.82	14.05	6.86	0.29	0.35	2.18	0.54	8.96
Rb	20	14	60	50	61	29	64	15	15	66	31	49
Sr	1 080	849	928	853	830	591	761	926	796	548	489	850
Th	4.82	1.68	2.14	1.70	2.48	2.91	5.97	1.99	1.66	1.99	1.45	1.93
U	1.75	0.63	0.93	0.60	1.11	0.81	1.70	0.63	0.52	0.70	0.52	0.67
V	61	101	132	175	156	261	134	96	100	181	194	306
Ga	18.5	18.8	15.6	17.5	15.5	16.4	18.2	18.8	18.4	16.1	13.2	15.4
Nb	19.3	4.5	2.9	3.2	3.5	3.5	6.3	5.4	4.2	3.0	1.6	2.8
Ta	1.1	0.2	0.1	0.1	0.2	0.2	0.3	0.2	0.2	0.1	0.1	0.1
Zr	151	72	72	76	103	69	120	90	69	75	61	52
Hf	3.4	2.0	2.0	2.1	3.2	1.9	3.1	2.2	2.0	2.1	1.9	1.6
Y	9.6	7.1	9.5	13.3	12.7	16.9	17.8	8.1	6.8	13.6	15.9	16.3
La	31.7	13.1	11.4	10.9	11.6	14.7	21.8	17.9	11.7	12.6	7.8	9.8
Ce	55.6	23.5	21.7	21.7	23.6	28.6	40.8	33.4	21.5	24.5	16.1	20.7
Pr	6.33	2.99	2.73	3.00	3.21	3.84	5.19	3.96	2.57	3.32	2.27	2.87
Nd	21.8	11.0	11.0	12.1	13.0	16.5	20.0	15.4	10.2	13.4	10.1	13.4
Sm	3.45	2.36	2.45	2.83	2.900	3.58	4.41	2.99	1.88	3.23	2.59	3.24
Eu	1.13	0.68	0.86	0.95	0.99	1.10	1.38	0.96	0.77	0.97	0.82	1.10
Gd	2.38	1.75	2.17	2.61	2.95	3.64	4.03	2.08	1.61	2.97	2.74	3.34
Tb	0.37	0.22	0.33	0.38	0.44	0.52	0.55	0.26	0.24	0.47	0.45	0.52
Dy	1.81	1.35	1.71	2.43	2.22	3.04	2.98	1.36	1.29	2.58	2.94	2.83
Ho	0.36	0.26	0.33	0.51	0.47	0.64	0.68	0.30	0.26	0.52	0.64	0.60
Er	1.03	0.73	1.07	1.48	1.36	1.84	1.59	0.80	0.62	1.25	1.87	1.68
Tm	0.12	0.13	0.15	0.20	0.21	0.26	0.26	0.11	0.07	0.23	0.28	0.24
Yb	0.89	0.60	1.07	1.45	1.45	1.65	1.71	0.71	0.59	1.37	1.86	1.76
Lu	0.15	0.11	0.18	0.22	0.23	0.26	0.26	0.09	0.10	0.21	0.28	0.23
Cu	29	45	46	59	97	133	45	11	11	55	88	95
Pb	5	<2	4	<2	30	4	34	<2	<2	<2	2	<2
Zn	59	50	39	27	190	85	77	55	53	48	66	75
Ni	13	11	29	20	20	20	7	17	9	19	53	53
Co	8	12	16	18	18	28	14	13	12	19	25	32

chromatography, and measured on a Thermo Fisher Scientific Triton Plus multi-collector thermal ionization mass spectrometer at Institute of Geology and Geophysics, Chinese Academy of Sciences (IGGCAS). The procedure blank was lower than 300 pg for Rb-Sr and 100 pg for Sm-Nd. The isotopic ratios are corrected for mass fractionation by normalizing to $^{88}Sr/^{86}Sr=8.375\ 209$ and $^{146}Nd/^{144}Nd=0.721\ 9$, respectively. The certified international standards, NBS-987 ($^{87}Sr/^{86}Sr=0.710\ 250\pm0.000\ 021$, $n=9$) and JNdi ($^{143}Nd/^{144}Nd=0.512\ 118\pm0.000\ 014$, $n=9$), were employed to test instrument stability during data collection. USGS CRM BCR-2 was measured to monitor the accuracy of the analysis protocol; the results are: $^{87}Sr/^{86}Sr=0.705\ 028\pm0.000\ 012$ and $^{143}Nd/^{144}Nd=0.512\ 635\pm0.000\ 014$. The $^{87}Sr/^{86}Sr$ and $^{143}Nd/^{144}Nd$ data on BCR-2 are in good agreement with previously published TIMS and MC-ICP-MS data (Li et al., 2012a, b).

3 PETROGRAPHY

These subvolcanic rocks are dominantly dacite, trachyte, andesite, trachy-andesite, and basaltic andesite. The textures of andesitic rocks are aphanitic to microcrystalline groundmass with locally granular; and trachytic, porphyritic, and glomeroporphyritic textures for dacitic rocks. The rocks are gray to grayish-green in color and predominantly consist of plagioclase, amphibole, and pyroxene in the groundmass and variably sized phenocrysts (Fig. 4), with accessory biotite, apatite, and iron oxides. Locally developed secondary phases are calcite, sericite, chlorite, epidote, and iron oxides and hydroxides. Amphiboles are normally zoned pargasite to magnesian hastingsite typically

with some oscillatory zoning (Yousefi et al., 2017b). These amphiboles have a common feature of opacitization. Pyroxene phenocrysts vary from augite towards diopside. Crystallization temperatures and pressures have been yielded from the phenocrysts compositions (see Yousefi et al., 2017b).

4 RESULTS
4.1 Whole-Rock Geochemistry

Whole-rock lithogeochemical data for the selected 12 subvolcanic igneous samples from the TAMB are listed in Table 1. Based on the Zr/TiO_2 vs. SiO_2 diagram (Fig. 5a), the rocks are classified as basaltic andesite, andesite, and dacite. And these rocks have a calc-alkalic and high-K calc-alkalic affinity (Fig. 5b). The primitive-mantle normalized trace element distribution (Figs. 5c, 5d) exhibits the enrichment in LILE (large ion lithophile elements) and LREE (light rare earth elements), depletion in HFSE (high-field strength elements), positive anomalies of K, Sr, Rb, and Ba, and negative anomalies of Nb and Ti. According to Özyurt and Altunkaynak (2020), these distinct geochemical features indicate the process of magma mixing and fractional crystallization.

These TAMB subvolcanic rocks are plotted within the adakite fields based on the MgO vs. SiO_2 (Fig. 6a), Sr/Y vs. Y (Fig. 6b), and $(La/Yb)_N$ vs. Yb_N (Fig. 6c) diagrams. They can be divided into two groups: the HSA (high-silica adakite) group in the Ahmad Abad region and the LSA (low-silica adakite) group in the Torud region. Other details of the lithogeochemical interpretation of these rocks are presented in Yousefi et al. (2017a). Since
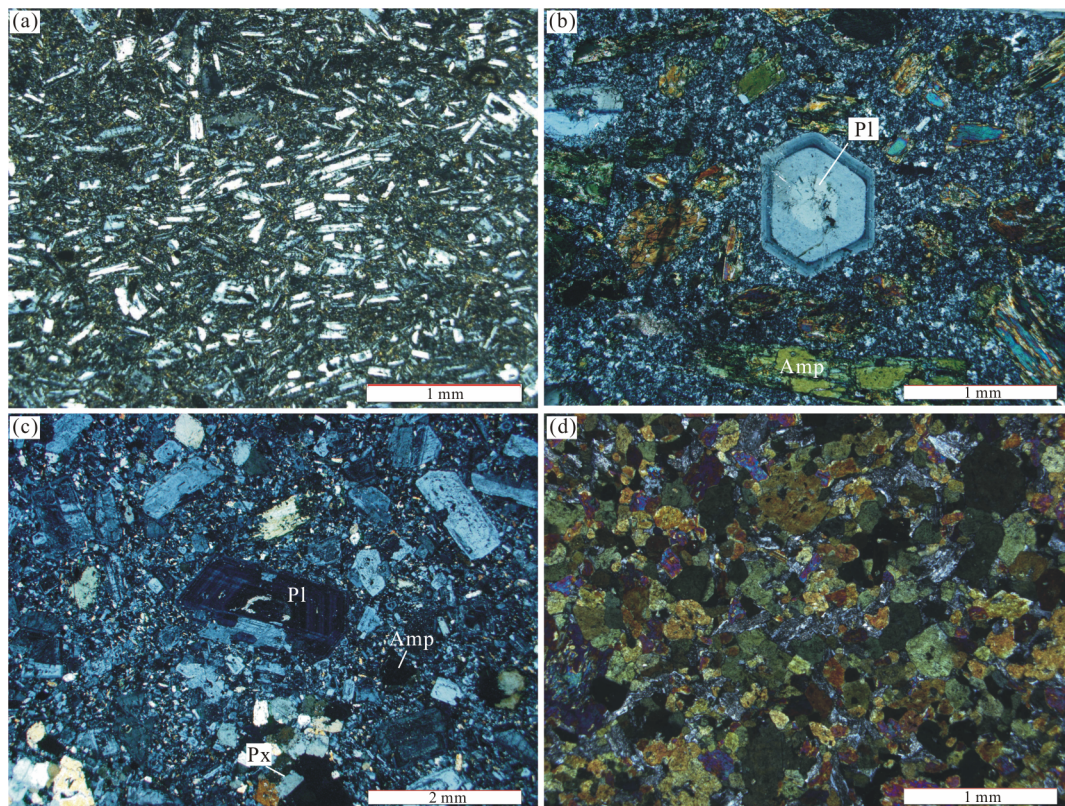
Figure 4. Photomicrographs showing the micro-characteristics of the TAMB adakitic rocks. (a) Trachytic textures consist of amphibole (Amp) and plagioclase (Pl) phenocrysts (PPL); (b) zoned plagioclase phenocryst with amphibole in porphyritic andesite (CPL); (c) accumulation of clinopyroxene (augite) phenocryst with zoned plagioclase (CPL) and (d) opacitized amphibole minerals in basaltic andesite (CPL). Mineral abbreviations are from Whitney and Evans (2010). Px. Pyroxene.

the main purpose of this paper is to present the new radiogenic isotopic results, therefore we abbreviated the explanation of the lithogeochemical studies. Finally based on the new data, we present a revised petrogenetic model and elaborate on the implications for enhancing the interpretation of the geodynamic setting.

4.2 Sr and Nd Isotope Geochemistry

Whole-rock Sr and Nd isotopic compositions and ε_{Nd} values of subvolcanic rocks from the TAMB are presented in Table 2. The initial Nd and Sr isotopic ratios and ε_{Nd} values were calculated using the 41.4 Ma age for the dacitic rock and 35.5 Ma age for the andesitic rocks. Detailed age determinations are presented in Yousefi et al. (2017a). The ε_{Nd} for these samples ranges from 3.7 to 6.0. These samples have Nd two-stage

model ages (T_{DM2}) of 0.34 to 0.53 Ga (see Table 2).

5 DISCUSSION
5.1 Magma Genesis and Evolution

In this section, we refer to the various factors affecting the geochemical signatures and isotopic features, such as fractional crystallization (FC) and assimilation-fractional crystallization (AFC) in the evolution of the magmas of this region (TAMB). A negative correlation between both Fe_2O_3 and TiO_2 with SiO_2 is consistent with FC of clinopyroxene and hornblende during the crystallization and the dispersion and deviation of Na_2O to SiO_2 of the linear process can be attributed to changes in the degree of partial melting or alteration of samples (Rollinson, 1993). The trends of Ho vs. Y represent the role of FC on
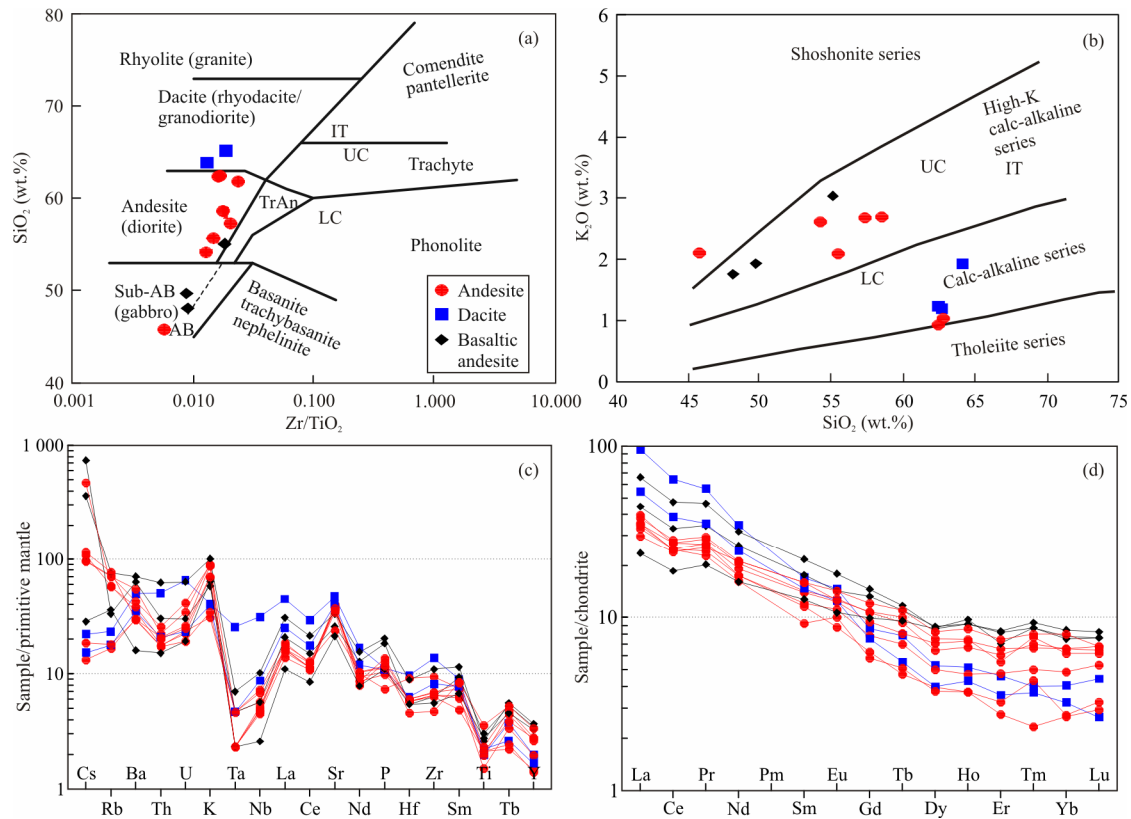

Figure 5. (a) Classification of subvolcanic rocks of the Torud-Ahmad Abad magmatic belt in terms of Zr/TiO_2 vs. SiO_2. These rocks plot within the range of basaltic andesite, andesite, and dacite (Winchester and Floyd, 1977). (b) The studied samples are plotted in the range of calc-alkaline (diagram after Peccerillo and Taylor, 1976). (c) Primitive mantle-normalized multi-element patterns of subvolcanic rocks of the TAMB (Wood et al., 1979). (d) Chondrite-normalized REE diagram (normalized values from Nakamura, 1974). UC. Upper crust; LC. lower crust; IT. I-type; average major and trace elements composition of various felsic rocks type in UC and LC after Wedepohl (1995), and IT after Whalen et al. (1987) and Pearce et al. (1984). Black diamond. basaltic andesite; blue square, dacite; red circle. andesite. Symbols are the same in all the following figures.

Table 2 Sr and Nd isotopic compositions of the studied sampled of Eocene hypabyssal rocks in the TAMB

Sample No.	FY-2-2	FR-6	FY-7a	FR-26	FR-32	FR-20*	FR-22*	FR-28*	FY-33*	FR-63*	FY-7b*
SiO_2 (wt.%)	59.8	45.5	61.6	53.6	45.0	55.9	53.0	53.5	62.0	56.8	61.6
$^{87}Sr/^{86}Sr_{(i)}$	0.703 886	0.704 62	0.703 868	0.704 794	0.705 314	0.704 599	0.703 833	0.704 079	0.703 746	0.704 227	0.703 854
$^{143}Nd/^{144}Nd_{(i)}$	0.512 819	0.512 789	0.512 865	0.512 857	0.512 775	0.512 821	0.512 787	0.512 825	0.512 775	0.512 811	0.512 893
$^{147}Sm/^{144}Nd$	0.095 6	0.131 0	0.117 0	0.145 0	0.146 0	0.135 0	0.095 3	0.135 0	0.113 4	0.126 5	0.108 0
$\varepsilon_{Nd(i)}$	+4.57	+3.97	+5.45	+5.30	+3.70	+4.60	+3.94	+4.67	+3.69	+4.41	+6.00
T_{DM2} stg (Ga)	0.46	0.50	0.39	0.40	0.53	0.46	0.51	0.45	0.53	0.47	0.34

Samples marked with stars from China and non-star samples from North Carolina.
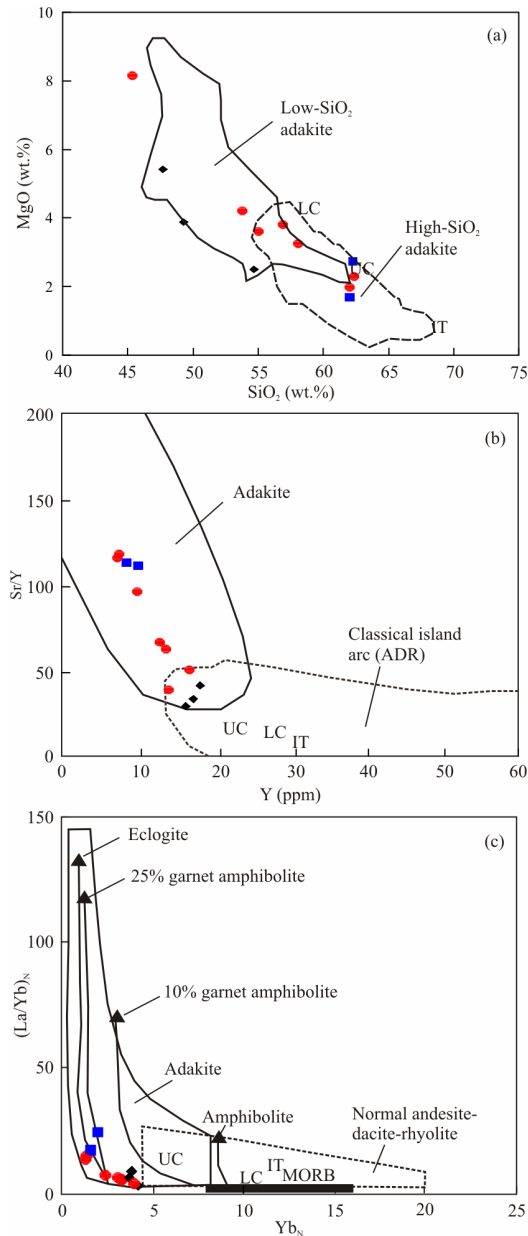
Figure 6. Geochemical classification diagrams for the adakite rocks in TAMB. (a) SiO_2 *vs*. MgO for discrimination of the high silica adakite (HSA) and low silica adakite (LSA) (after Castillo, 2012), low-silica adakites in the Torud region and high-silica adakites in Ahmadabad region; (b) Y *vs*. Sr/Y (after Defant and Drummond, 1990); (c) $(La/Yb)_N$ *vs*. Yb_N (after Defant and Drummond, 1990). See Fig. 5 for other symbols (UC, LC, IT).

magma evolution. Low deflection of linear values are attributed to the degree of partial melting. Therefore, based on enrichment in LILE and LREE in a depleted source, the role of partial melting in the production of this magma is clear. In this study, the K_2O/Na_2O *vs*. Rb/Zr ratios were chosen for illustrating the important role of the combination of fractional crystallization with assimilation (AFC) on the evolution of the magma producing the TAMB subvolcanic rocks. Lucci et al. (2016) demonstrated the importance of differentiation in evolution of calc-alkaline magmatic suites of Sabzevar region, which is adjacent to TAMB.

Murphy (2007) suggested that intermediate and felsic rocks can originate from fractional crystallization of a more mafic parent magma because the early fractionation of olivine, clinopyroxene, and plagioclase drives the liquid to more silicic compositions. To investigate crustal contamination, the element ratios of Rb/Y *vs*. Nb/Rb (Fig. 7) are used. Vertical trends in this diagram indicate enrichment in relation to subduction and crustal contamination (Temel et al., 1998). Based on the observed trends, the presence of various enclaves, and petrographic disequilibrium and reaction textures, the magmas forming the subvolcanic rocks TAMB are suggested to have evolved by magma mixing (Yousefi et al., 2017a, b). Changing the environment during the ascent of magma leads to changes in textures and minerals, e.g., zoning and opacitization. According to Wallace and Bergantz (2002) zoning in crystals progressivley recorded changes in the magmatic environment and it records physical and chemical changes in the magmatic liquids from which the crystals grow. The opacitization is due to an imbalance of hydrous minerals in an anhydrous, high temperature environment under the influence of exothermic processes and dropping pressure (Middlemost, 1986). The ratio of Th/U has also been used to determine the role of crustal contamination (Rudnick and Gao, 2003) in the evolution of the studied rocks. The Th/U ratio of the crust and of the studied rocks is 3.80 and 2.00 to 3.95, respectively. Furthermore, the ratio of Rb/Nb is high in these rocks (1.03–22.1), suggesting a subduction-related environment (Yousefi et al., 2017a, b). Based on Zheng (2019), strong thermal and chemical disequilibrium have been generated by subduction, causing to dehydration and hydration, mineral transformations, and partial melting of crustal and mantle rocks.

One of the interesting topics that has been considered recently is the link between adakite and TTGs. First, various theories about the genesis of adakites and the TTGs are presented. Moyen and Martin (2012) presented four models for the origin of TTGs. (1) Fractional crystallization of a wet basaltic magma, although Archaean cratons include mafic rocks, geochronology studies show that the basalt and TTG are rarely coeval. This model is proposed for similar group of rocks called adakites. In this group, amphibole and garnet play an important role in fractional crystallization. But the role of garnet is obvious in creating the typical HREE depletion in adakites/TTGs. According to Moyen (2009), the fractional crystallization process is undoubtedly able to generate some high Sr/Y or La/Yb magmas. (2) Mantle melting and the role of fluid in mantle metasomatised (Peterman and Barker, 1976), they believed that low degree of melting required to generate felsic magma. (3) Partial melting of Archaean greywackes, according to Martin (1994), this model does not justify the major- and other trace-element behavior. (4) Partial melting of a hydrated basalt metamorphosed at high pressure and transformed into eclogite or garnet-bearing amphibolite, in this model, it is accepted that garnet is stable in the residue and it is the reason for the depletion of the HREE within TTG.

At the end of 1980s, a model was accepted for the TTG genesis, which includes these items (Martin, 1994): (1) partial melting of the mantle to produce a basalt; (2) melting of the basalt, metamorphosed to garnet bearing eclogite or amphibolite, to produce the parent magma of TTG; (3) low pressure fractional crystallization to produce the differentiated TTG groups.
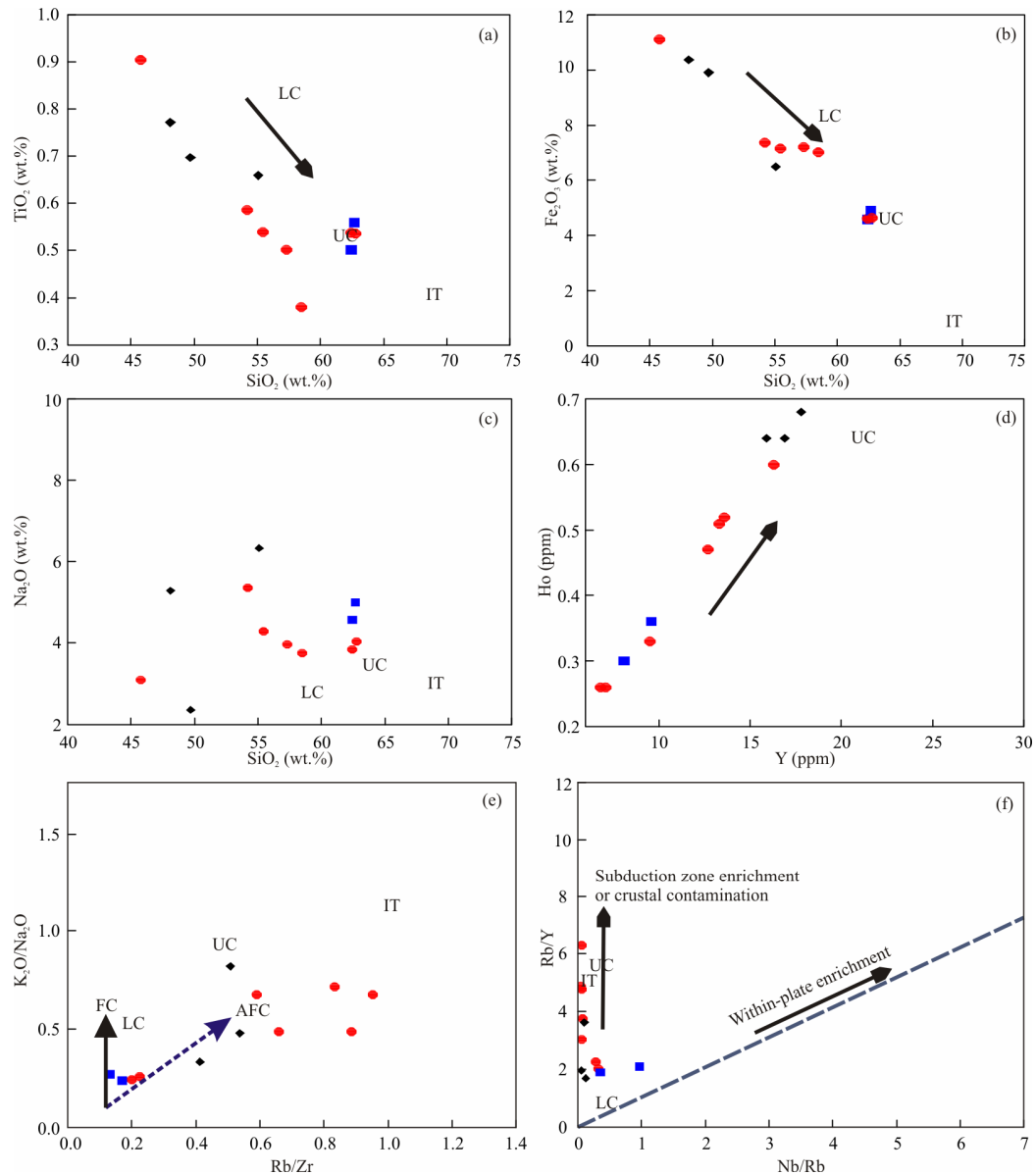
Figure 7. Harker diagrams (a)–(d) of subvolcanic rocks of the TAMB (after Harker, 1909); (e) K₂O/Na₂O *vs.* Rb/Zr and (f) Rb/Y *vs.* Nb/Rb compositional systematics of subvolcanic TAMB rocks. These diagrams show the fractional crystallization (FC) with assimilation and fractional crystallization (AFC) on the evolution of the magma producing the subvolcanic rocks. See Fig. 5 for other symbols (UC, LC, IT).

According to Defant and Drummond (1990), adakite is known as a modern arc lavas. As in the Moyen and Martin (2012) article, the two definitions of TTG and adakite are the same. This comparison was based on the chemical composition and similarity between the two groups such as the high La and Sr, low Y and Yb contents, and correlated high Sr/Y and La/Yb ratios. The definitions of these groups state that both are in an arc environment and are calc-alkaline in nature. These features have also been proven in the adakites we studied. Given the geochemical similarities between adakites and TTG, it has been suggested that they formed by very similar processes (Martin et al., 2005).

Since adakites are formed in the subduction environment, they are considered as a sign in the subduction environment and therefore it can be concluded that the TTG are also related to the subduction environment. Kusky et al. (2018) believed that when subduction of oceanic plates happen, they return to the

mantle in a cycle. Dehydration of the subducted plate at a depth of 110–200 km helps partial melting of the mantle, and this melting leads to the production of a magmatic arc.

Martin et al. (2005) believed that only in some characteristics are there differences between the TTG and low silica adakitic (LSA) magmas. But after studying the geochemical properties, they came to the conclusion that the TTG is most similar to high silica adakite (HSA).

According to geochemical and isotopic studies, these rocks are the result of melting of the oceanic sheet and consequently mantle metasomatism. According to Mathieu and Racicot (2019), mantle metasomatism causes the production of magma, which is involved in mineralization in subduction environments. We found this evidence of mineralization in parts of Central Iran such as Sarcheshmeh porphyry Cu deposit. Based on Boomeri et al. (2010), hydrothermal activity related to a subvolcanic Miocene

granodiorite stock plays an important role in the production of the Sarcheshmeh porphyry Cu deposit. Moyen (2009) believed that adakites are arc rocks and are observed in subduction environments, and it happens when a hot, young oceanic lithosphere is subducted. As mentioned several times in the text, the adakitic rocks of the study area are the result of subduction of young Neo-Tethys oceanic slab and mantle metasomatism.

5.2   Tectonic Setting and Magma Source Region

Based on the element ratios Th/Yb *vs*. Nb/Yb (Th/Nb ratios, Fig. 8; Pearce, 2014) and Th/Ta (Gorton and Schandl, 2000), the studied samples plot in the volcanic arc array and the upper part of the OIB and N-MORB. Nicholson et al. (2004) suggested that enrichment of LREE and LILE with depletion of HREE (heavy rare earth element) and HFSE (high field strength element) is one of the important features of arc magmatism in a subduction environment. According to Li et al. (2015), high Sr/Y and Sr/Yb ratios are associated with subduction zones. Chiaradia (2009) noted that the existence of andesitic to dacitic rocks in arc regions with high Sr/Y and low HREE are indicative of melting of a subducted slab. The negative Nb and Ti anomalies suggest that these rocks have been produced in relation to the subduction of oceanic crust below the continental crust. Examining the sediments, Plank (2014) explained that the arcs regions inherit the anomaly of Nb directly from the sediments, or are a sign of the remaining rutile in the slab. In a subduction zone, fluids released from the sub-

ducted oceanic lithosphere, which is rich in LILE, are added to the mantle wedge (Eyuboglu et al., 2011; Borg et al., 1997; Gill, 1981). Their low Y and HREE contents indicate that garnet was an important phase in the residuum assemblage (Eyuboglu et al., 2012). During rapid magma ascent through the subcrustal (continental) lithospheric mantle (SCLM) and continental crust, processes such as FC and AFC may affect the evolution of the magma (Sheth et al., 2002). In a previous study by Yousefi et al. (2017a), the presence of mantle and crustal enclaves was shown to illustrate the possible role of crustal contamination in the evolution of these magmatic systems; subduction erosion of the accretionary complex can also produce isotopic signatures resembling crustal contamination. Also Yousefi et al. (2017b) investigated the depth of source magma chambers through geothermobarometric calculations based on the phenocryst compositions in rocks and enclaves.

The whole rock two-stage Nd model ages (0.34–0.53 Ga) suggest the source of lithospheric mantle and crust (interaction of oceanic crust and continental crust during the melting of oceanic crust) for rocks in TAMB (Yousefi et al., 2017a). As mentioned in the above sections, there are two rock types of adakites in this region, high silica adakite (HSA) and low silica adakite (LSA) (Figs. 6, 7). The source of LSA is partial melting of mantle that is modified by fluids released from subducted oceanic crust, and HSA are due to the melting of oceanic crust that interacts with continental crust. Similar findings have been presented by Karsli et al. (2013) from the eastern Pontides (NE
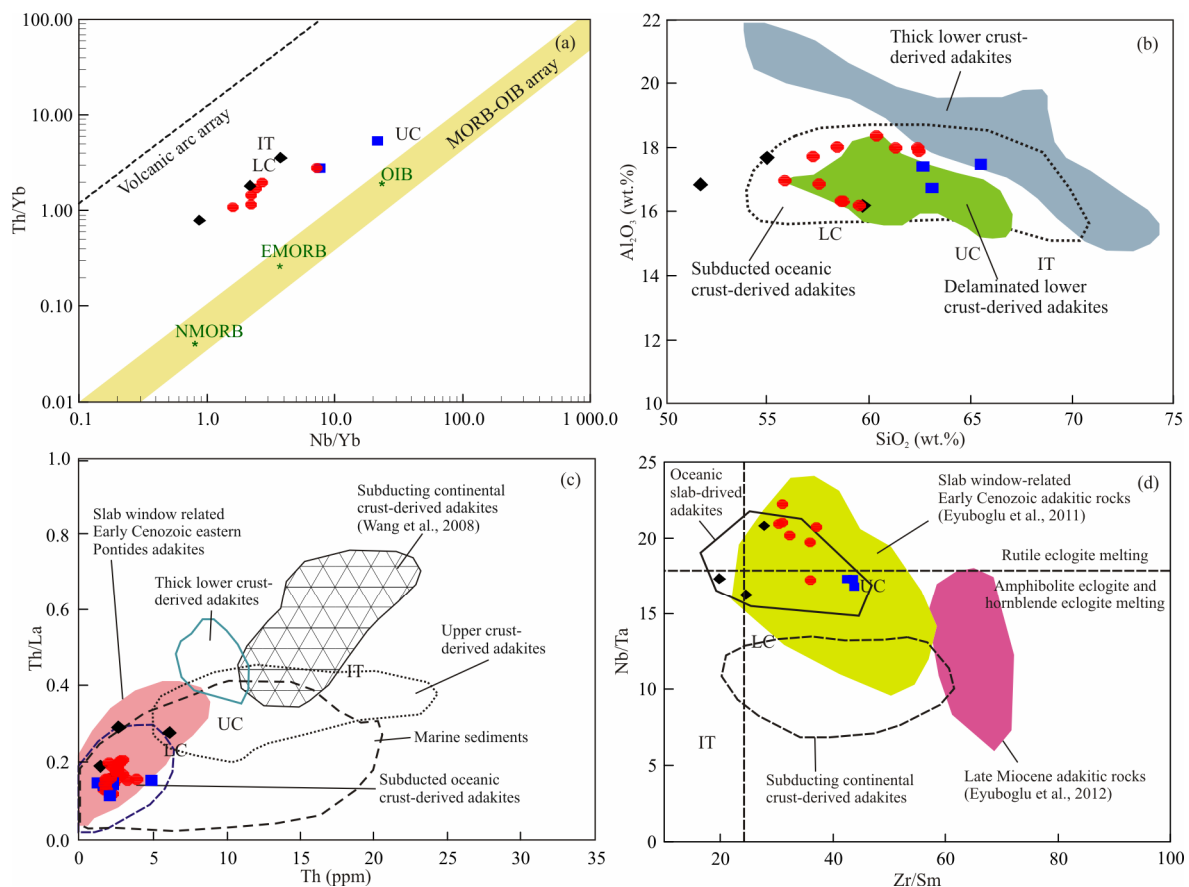
Figure 8. Discrimination diagrams for TAMB rocks. (a) Nb/Yb *vs*. Th/Yb (Pearce, 2014); (b) and (c) Al$_2$O$_3$ *vs*. SiO$_2$ and Th/La *vs*. Th (Wang et al., 2008); (d) Nb/Ta *vs*. Zr/Sm diagram (Eyuboglu et al., 2012).

Anatolia). Rare earth elements variations and MgO and SiO_2 contents indicate that fractional crystallization or partial melting played a role in their genesis.

Castillo (2006) suggested that the formation of HSA is due to subducted oceanic slab with the role of fractional crystallization and assimilation (AFC). Based on petrological and geochemical studies on arc magmas, the role of fractionation (FC and RFC: replenishment-fractional-crystallization) and fractional crystallization and assimilation (AFC) appeared (Lucci et al., 2016). With respect to Martin et al. (2005), HSA are interpreted as a result of melting of oceanic slab with the composition of garnet-amphibolite at a pressure equal to the range of garnet stability. According to Fig. 6c, garnet amphibolite must be a residuum and adakite melt source. Some of the samples plotted in eclogite range (LSA). It is clear that the source of these adakite melt is eclogite at greater pressure that garnet amphibolite. Hastie et al. (2010) suggested that Cenozoic adakites are derived from high pressure (>1 GPa) and approximately 20% partial melting of amphibolite, garnet amphibolite or eclogite source regions.

The melt that creates the HSA changed while crossing mantle wedge. In these melts, when uplift and interaction with mantle occurs, the composition of the major elements changes, but other characteristics, such as the ratio of rare earth elements show less changes (Mori et al., 2007). The LSAs (basaltic andesites and andesites in Sahl-Razzeh region) have been sourced from an enriched mantle that was modified with the fluids released from a metamorphosed subducted oceanic slab.

Partial melting of the peridotitic mantle wedge, with the role of fluids released from metamorphosed subducted oceanic slab, can lead to the formation of andesite as a result of melting of a subducted slab with a high amount of Sr/Y and low amount of HREE. These features have been considered to indicate direct melting of subduction slab (Chiaradia, 2009), and yields an adakitic magma with low silica content (Davies and Stevenson, 1992). Moyen (2009) suggested that HSA is the result of the melting of subducted oceanic slab at a depth of about 80 km below the surface of the earth and LSA is the result of partial melting of a modified mantle above the subducted oceanic slab at a depth of 50 to 60 km. The generated magma moves rapidly upwards and is emplaced into the upper crust. Due to the existence of different types of cogenetic and non-cogenetic enclaves, incorporated during the magma ascent, constructor magma of these studied rocks have evolved under the influences of processes, such as FC and AFC. To investigate the origin of adakitic rocks in the studied area, we used the concentrations of Al_2O_3 vs. SiO_2 and Th/La vs. Th in the diagrams of Wang et al. (2007). According to these diagrams, these TAMB subvolcanic rocks plotted in the range of subducted oceanic crust-derived adakites (Fig. 8). Based on Yumul et al. (2017), the mechanism of formation for adakitic rocks has been extended to contain lower crust melting, slab melt-mantle interaction, high pressure fractionation, possibly with sediment melting (subduction erosion) and ridge subduction, among others.

By using the results from radiogenic isotope analysis and petrogenetic diagrams, the origin of the studied rocks can be identified. Based on the equations and average ages of samples (Yousefi et al., 2017a), the initial isotopic ratio of Nd and Sr

has been calculated. According to the results, isotopic characteristics of the 12 studied samples correspond to the melting of subducted oceanic slab and partial melting of modified mantle. Initial ratio values of $^{143}Nd/^{144}Nd$ are in the range 0.512 775 to 0.512 893 and initial ratio values of $^{87}Sr/^{86}Sr$ are in the range of 0.703 746 to 0.705 314. The $\varepsilon_{Nd(i)}$ values for these rocks are high and positive (+3.69 to +6.00). Based on $\varepsilon_{Nd(i)}$ vs. $^{87}Sr/^{86}Sr_{(i)}$, these adakitic rocks in this magmatic belt are in the range of subducted slab-derived adakitic rocks with relatively high $\varepsilon_{Nd(i)}$ and low $^{87}Sr/^{86}Sr$ ratios (Fig. 9). In fact, positive values indicate a slight depletion at the source to the chondritic reservoir (CHUR) at the time of their formation. This indicates the influence of the mantle in the formation of these rocks (Zindler and Hart, 1986). The range of subducted slab-derived adakitic rocks has been defined by Defant et al. (1991). The studied samples of the TAMB area overlap with the range of Eocene adakitic rocks of Pontide (Eyuboglu et al., 2011) that are related to subducted oceanic lithosphere. These adakitic rocks were associated with a subducting oceanic slab that is related to convergent margins, although to preserve these primitive mantle isotopic signatures they would need to have a low residence time ascending through the SCLM and continental crust. The data of classical adakite and continental adakite rocks were compiled by Chung et al. (2003), He et al. (2013), Xu et al. (2002), Ma et al. (2015), and Rapp and Watson (1995).

For a more detailed study of the petrogenesis of LSA, the LSA data was separated from the HSA data. According to the diagram of initial $^{87}Sr/^{86}Sr$ vs. initial $^{143}Nd/^{144}Nd$ ratio, the LSA with a composition of basaltic andesite and andesite from Sahl-Razzeh region, is derived from the mantle that has been modified by the fluids released from the subducted Sabzevar Neotethian oceanic slab (Fig. 10). The data for eastern Anatolian CAV (calc-alkaline volcanic rocks) were presented by Temizel et al. (2012) and Kaygusuz et al. (2011) and the data for eastern Pontide were presented by Keskin et al. (2006) and Kaygusuz (2009). Based on the diagram of $^{87}Sr/^{86}Sr_{(i)}$ vs. $\varepsilon_{Nd(i)}$, the LSA in this region is the result of melting lithospheric mantle. These samples come from the Sahl-Razzeh region (Fig. 10). Now, we
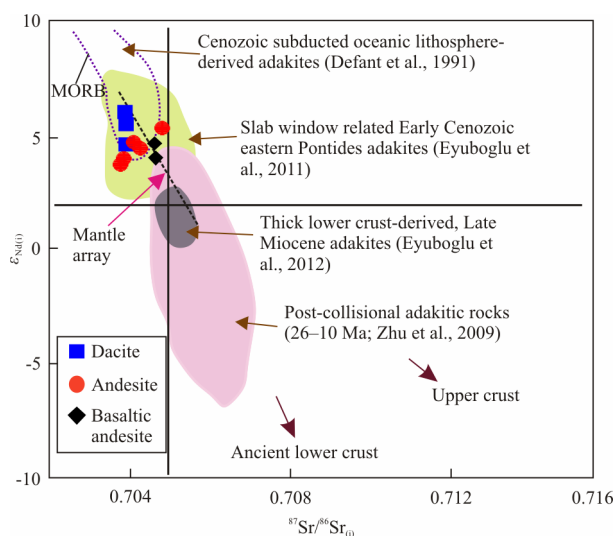
Figure 9. Diagram of $\varepsilon_{Nd(i)}$ versus $^{87}Sr/^{86}Sr_{(i)}$ for the Eocene to Middle Eocene adakitic rocks from the Torud-Ahmad Abad magmatic belt.

look at the role of the contribution of sediments (subduction erosion) along with the melting of the subducted oceanic slab, in the development of magma-forming of this magmatic belt. The variation diagrams of Cs/Th *vs*. La/Sm (Jenner and O'Neill, 2012), the Th/Yb *vs*. Th/Sm (Sun and McDonough, 1989) and Yb *vs*. Th/Ta (Gorton and Schandl, 2000) (Fig. 11) illustrates the influence of the derivative magma from subducted sediments together with the subducted oceanic slab; they are clearly demonstrated, i.e., the crustal like radiogenic isotopic signatures do not reflect assimilation of continental crust, supporting a short residence time (rapid) during emplacement consistent with local extension. According to Pearce and Peate (1995), Th is a HFSE, but it is a non conversative element in arc regions. Gorton and Schandl (2000) believed that abundance and solubility of Th in subduction zone is very low and this element was derived from a sediment component of the subducted slab. Although the exact mechanism of enrichment of Th with respect to Ta is debatable, in arc magmas the ratio of Th/Ta is higher than magmas generated in within-plate volcanic zones.

5.3 Tectonic Events in the Northern Central Iran Zone

Berberian and Berberian (1981) stated that tectonic activity in Iran includes several generations of deformation. One important event is the subduction of the Neo-Tethys oceanic slab under the Central Iran Plate (Ahmadian et al., 2014; Stampfli and Borel, 2002). This tectonic event led to intrusive and volcanic activity in the Central Iran zone (Mohajjel et al., 2003; Ricou et al., 1977). The convergence of the Arabian and Eurasian plates created back-arc basins in the Central Iran zone, with subduction of the Neo-Tethys oceanic slab (the branch of Sabzevar) continued during the Cretaceous. Collision of Arabia and Eurasia occurred between 10 to 20 Ma (McQuarrie et al., 2003). Azizi et al. (2011) pointed to the adakitic magmatic units in northwestern Iran and in the northern part of the Urumieh-Dokhtar belt, which were affected by the subduction of the Neo-Tethys oceanic plate. According to Moghadam et al. (2016) and Lucci et al. (2016), Eocene adakitic rocks in northern Sabzevar in the area adjacent to TAMB are also the result of the subduction of the Neo-Tethys oceanic plate. They have suggested this tectonic event was induced by magmatic "flare-up" in this part of Iran, which is also consistent with an extensionally event in an formerly arc building environment.

In Central Iran, a local oceanic basin opened at the beginning of the subduction cessation, whereas the subduction of the Sabzevar branch continued. The existence of *Muricohedbergella Planispira* and *Whiteinella Archaeo Cretacea* fossils in this part of Iran indicates an Upper Cretaceous age for the sedimentary basin of some parts of the Central Iran zone, especially Sabzevar (Yousefi, 2017). If subduction continued, evidence of continental margin magmatism and locally extensional (intra-arc rifting) is clear. According to Hamilton (1988) and Lentz (1998), there is evidence that show all transitional arc to back arc magmatism is extensional in nature, and that back arc development transitional from intra-arc rifting are principal characteristics of these transitional settings. Pirajno (2016) noted that the type of mineralization varies in each tectonic environment as well. For example in major intra-arc rifts, there is generation of massive sulphide deposits of Kuroko affinity. Transpression can cause slab windows, slab rollback, and slab breakoff that also can cause asthenosphere upwelling, in addition to SCLM and crustal local extension (leading to voluminous magmatism). The differences in degree of extension, tension or compression regime affect calc-alkaline *vs*. tholeiitic/alkalic magmatic evolutionary process (cf. Lentz, 1998). It should be mentioned that these events are associated with subduction and melt generating process, which occurs under the influence of upwelling and convention of the asthenospheric mantle. As mentioned above, strong evidence of extension in this area is enclaves that are composed of pyroxene and hornblende. Based on microprobe studies, these phenocrysts crystallized at >8 kbar (Yousefi et al., 2017b) and their compositions were preserved, consistent with rapid emplacement. The mantle and lower crustal xenoliths originated from fragmentation of rocks near the lithospheric crust-mantle boundary, where magma has brought them up (entrained) during a rapid ascent. Also, the other evidence of extension is the emplacement of this magmatic belt through the Neoproterozoic metamorphic units and Middle Jurassic low grade metamorphic rocks and their entrainment during ascent (Yousefi, 2017).

The mantle wedge above the subducted oceanic lithosphere was affected by dehydration of oceanic slab that melted and created the LSA. In other words, transpression (locally extensional) aids in slab melting and migration through the cooled (refrigerated)
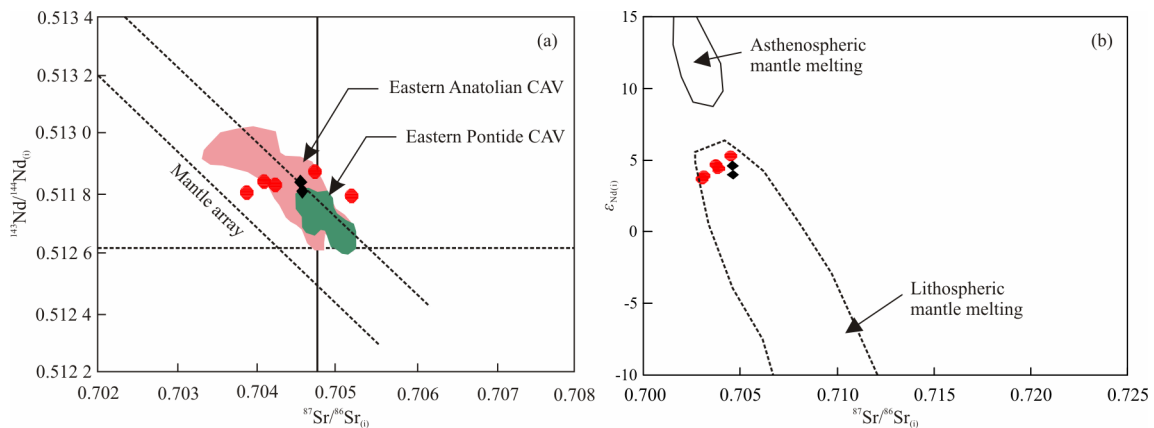
Figure 10. Diagrams for determining the origin of low silica adakite. (a) Diagram of initial $^{87}Sr/^{86}Sr$ *vs*. initial $^{143}Nd/^{144}Nd$ ratio (Temizel et al., 2012); (b) diagram of $^{87}Sr/^{86}Sr_{(i)}$ *vs*. $\varepsilon_{Nd(i)}$ from Zhang et al. (2016).
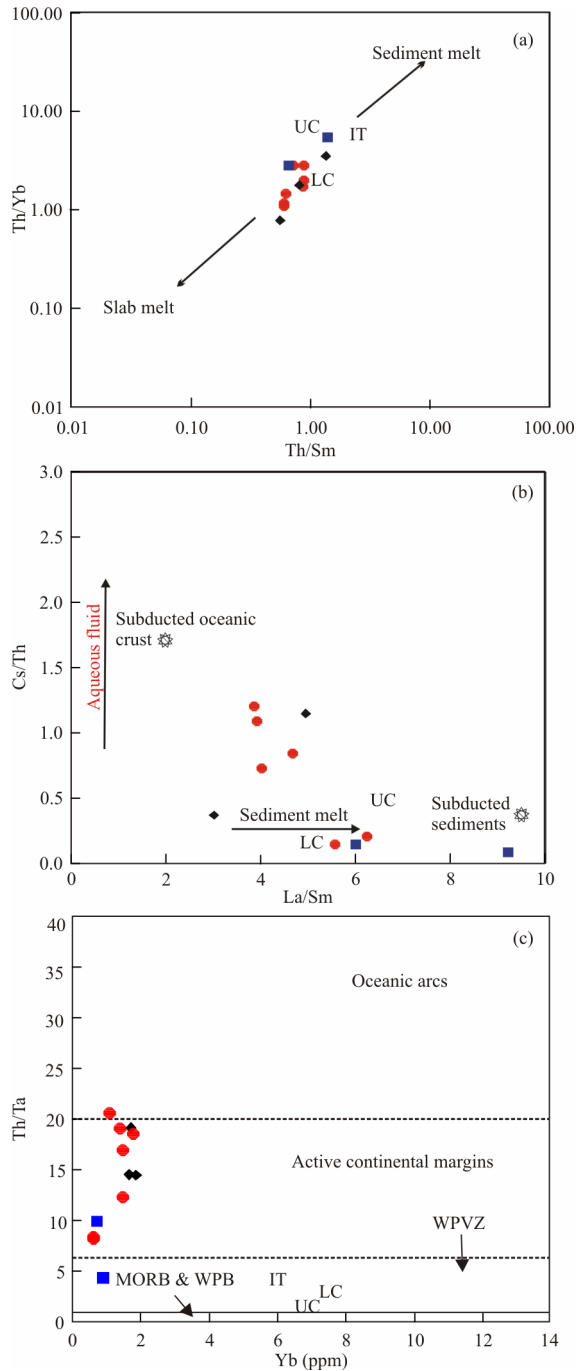
Figure 11. Diagrams of (a) Th/Yb *vs*. Th/Sm (Sun and McDonough, 1989) and (b) Cs/Th *vs*. La/Sm (Jenner and O'Neill, 2012). It can be revealed from these diagrams that the studied rocks have been affected by both the melting of the oceanic slab and the melting of its associated sediments. (c) Th/Ta *vs*. Yb discriminant diagram (Gorton and Schandl, 2000). The samples are plotted in the active continental margins. WPVS. Within-plate volcanic zones; WPB. within-plate basalts.

suprasubduction zone (SSZ) mantle then SCLM and crust. Hyndman et al. (2005) showed that in a few continental regions for example basin, crustal extension (thinning) has an additional thermal effect. Similarly in areas where extension occurred in the oceanic crust, it is difficult to distinguish the thermal effect of extension from that of convective heat transport in the underlying shallow asthenosphere. Even in these

basins, small-scale convection was needed for lithosphere thinning to occur. With continued subduction and melting of the hydrous oceanic slab in deeper sections, HSA was formed. During the subduction of hydrous oceanic slab, some parts of the slab might have failed and separated (Fig. 12). Based on the summary of all field and laboratory data, a schematic model of the Torud-Ahmad Abad magmatic belt is presented in Fig. 12. The model presents the dominance of a compressional tectonic regime and continuation of subduction of the Neo-Tethys oceanic slab in the Middle–Upper Cretaceous, opening of a sedimentary-volcanic basin reflecting an extensional regime (Late Paleocene–Early Eocene) (e.g., Ghasemi and Rezaei-Kahkhaei, 2015), melting of modified mantle under the influence of dehydration of subducted oceanic slab (LSA) (Fig. 12a), and continuation of subduction and melting of subducted oceanic lithosphere creating the acidic and intermediate magmas, emplaced as small subvolcanic intrusions or dikes (HSA) (Fig. 12b). Finally, it should be noted that although according to Verdel et al. (2011), in some parts of Iran, there is "flare-up", however, according to the geochemical evidence mentioned above, along with the isotopic evidence, this group of rocks in this part of Central Iran is from the subduction of the ocean lithosphere; this needs to be reconciled with extension-related flare-up. In intracrustal arc settings, if Nb element is not depleted, the presence of a "flare-up" is suspected (Verdel et al., 2011). But according to Fig. 5, the rocks examined in this area have depletion of Nb and Ta with relatively low Th and U (limiting the possibility of crustal contamination). Therefore, these separate adakitic rocks were not derived independently of upwelling asthenosphere (possibly due to slab rollback and (or) failure) unlike the terrestrial to marine Neogene rift basalts; heat advection and uplift (with extension) of the lithosphere and crust throughout the Late Eocene to Neogene would have caused widespread melting that is described as magmatic "flare-up" occuring in extensional settings. Hassanzadeh et al. (2004) described stratigraphic evidence of Eocene subsidence in the Alborz Mountains and Central Iran that has also been interpreted in terms of a transition to Eocene extension. The samples used by Verdel et al. (2011) were not adakitic samples, whereas this study specifically focused the adakitic rocks of this part of Central Iran zone to examine the array of arc-like extensional magmatism and specific timing relative to the earlier and later magmatic events. Based on U-Pb zircon dating, the ages of these two groups of rocks are 35.5±0.3 and 41.4±0.3 Ma, thus inferring a Middle–Late Eocene age for the transition to the transtensional geodynamic environment preceding overall extension and flare-up.

6 CONCLUSIONS

Geochemical results indicate that the subvolcanic rocks of Torud-Ahmadabad magmatic belt have the composition of dacite, trachyte, andesite, trachy-andesite, and basaltic andesite, and they plot in the volcanic arc array. The geochemical data of the studied rocks reveal that they have adakite to adakite-like geochemical features with a calc-alkaline nature.

Enrichment in LILE (large ion lithophile elements) and LREE (light rare earth elements) to HFSE (high-field strength elements), such as the negative Nb and Ti anomalies and positive
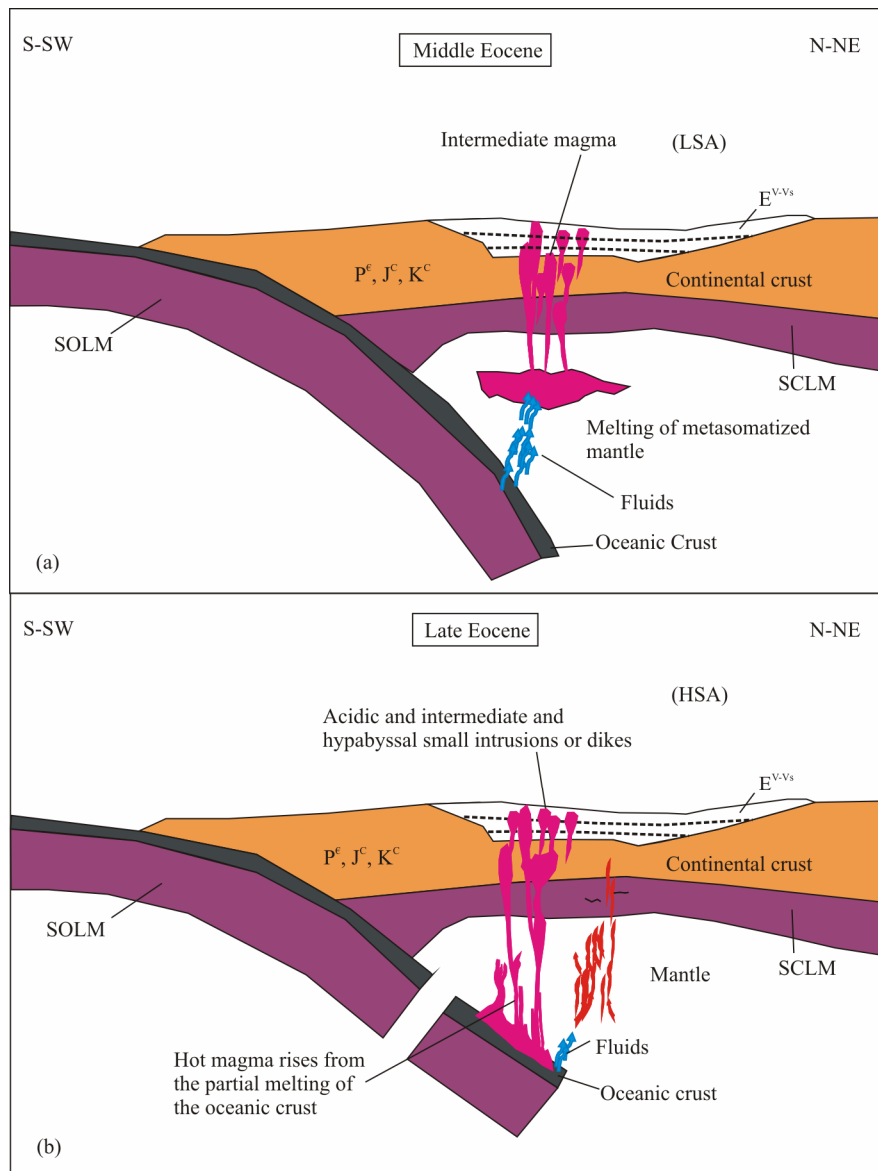
Figure 12. Schematic tectono-magmatic model of Torud-Ahmad Abad magmatic belt. (a) Opening of a sedimentary-volcanic basin with the rule of extensional regime (Late Paleocene–Early Eocene) and melting of the modified mantle under the influence of dehydration of subducted oceanic slab (LSA). (b) Continuation of subduction and melting of subducted oceanic lithosphere for creating the acidic and intermediate, and subvolcanic small intrusions or dikes (HSA). The abbreviations in these figures are: S-SW. direction south-southwest; N-NE. direction north-north east; E^{V-Vs}. Eocene volcanic and volcano-sedimentary; P^ϵ, J^C, K^C. Older rocks units to the Eocene (belong to Precambrian, Jurassic, Cretaceous); SCLM. subcontinental lithospheric mantle (uppermost solid mantle); SOLM. suboceanic lithospheric mantle.

K, Sr, Rb, and Ba anomalies refer to their formation related to the subduction of oceanic slab below continental crust. Thus the chemical disequilibrium is caused by the interaction of the oceanic crust and the mantle above the subducted slab. The enrichment in LILE and LREE and depletion in HREE suggest the existence of garnet amphibolite or eclogite in the source of these rocks during selective partial melting.

According to geochemical data and field observations, effective factors on subsequent magma evolution are fractional crystallization and sediment contamination from subduction erosion, and to only a minor extent crustal contamination due to rapid emplacement, i.e., low crustal residence time; this is consistent with xenoliths and preservation of high pressure hornblende phenocrysts.

Initial ratio values of $^{143}Nd/^{144}Nd$ are in the range 0.512 775 to 0.512 893 and initial $^{87}Sr/^{86}Sr$ ratios range from 0.703 746 to 0.705 314. The Sr-Nd isotope data show that the origin of low silica adakite (LSA) or adakite-like rocks reflect partial melting of modified mantle above the subducted oceanic slab and the origin of high silica adakitic (HSA) rocks formed by melting of subducted oceanic slab of Sabzevar branch of the Neo-Tethys.

Finally, by using Sr and Nd isotopic data along with whole-rock geochemistry and various field evidence, the source for these dominantly adakitic rocks of Torud-Ahmadabad magmatic belt is from a subducted Neo-Tethys oceanic slab and mantle metasomatism in the SSZ. The Late Eocene voluminous magmatism looks to be associated with local extension (transpression) in the continentally situated arc setting evolving to

rifting in the Neogene that maybe caused by slab rollback or breakoff coincident with upwelling asthenospheric mantle throughout this period.

ACKNOWLEDGMENTS

REFERENCES CITED

Ahmadian. J., Murata. M., Nadimi, A., et al., 2014. Recent Tectonic Activity of Iran Deduced from Young Magmatism Evidences. *Bulletin of Center for Collaboration in Community Naruto University of Education*, 28: 23–38

Azizi, H., Tanaka, T., Asahara, Y., et al., 2011. Discrimination of the Age and Tectonic Setting for Magmatic Rocks along the Zagros Thrust Zone, Northwest Iran, Using the Zircon U-Pb Age and Sr-Nd Isotopes. *Journal of Geodynamics*, 52(3/4): 304–320. https://doi.org/10.1016/j.jog.2011.03.001

Balaghi Einalou, M., Sadeghian, M., Zhai, M. G., et al., 2014. Zircon U-Pb Ages, Hf Isotopes and Geochemistry of the Schists, Gneisses and Granites in Delbar Metamorphic-Igneous Complex, SE of Shahrood (Iran): Implications for Neoproterozoic Geodynamic Evolutions of Central Iran. *Journal of Asian Earth Sciences*, 92: 92–124. https://doi.org/10.1016/j.jseaes.2014.06.011

Berberian, F., Berberian, M., 1981. Tectono-Plutonic Episodes in Iran. *Geological Survey of Iran*, *Report*, 52: 566–593

Boomeri, M., Nakashima, K., Lentz, D. R., 2010. The Sarcheshmeh Porphyry Copper Deposit, Kerman, Iran: A Mineralogical Analysis of the Igneous Rocks and Alteration Zones Including Halogen Element Systematics Related to Cu Mineralization Processes. *Ore Geology Reviews*, 38(4): 367–381. https://doi.org/10.1016/j.oregeorev.2010.09.001

Borg, L. E., Clynne, M. A., Bullen, T. D., 1997. The Variable Role of Slab Derived Fluids in the Generation of a Suite of Primitive Calc-Alkaline Lavas from the Southernmost Cascades: California. *Canadian Mineralogist*, 35: 425–452

Castillo, P. R., 2006. An Overview of Adakite Petrogenesis. *Chinese Science Bulletin*, 51(3): 257–268. https://doi.org/10.1007/s11434-006-0257-7

Castillo, P. R., 2012. Adakite Petrogenesis. *Lithos*, 134/135: 304–316. https://doi.org/10.1016/j.lithos.2011.09.013

Chiaradia, M., 2009. Adakite-Like Magmas from Fractional Crystallization and Melting-Assimilation of Mafic Lower Crust (Eocene Macuchi Arc, Western Cordillera, Ecuador). *Chemical Geology*, 265(3/4): 468–487. https://doi.org/10.1016/j.chemgeo.2009.05.014

Chung, S. L., Liu, D. Y., Ji, J. Q., et al., 2003. Adakites from Continental Collision Zones: Melting of Thickened Lower Crust beneath Southern Tibet. *Geology*, 31(11): 1021–1024. https://doi.org/10.1130/g19796.1

Davies, J. H., Stevenson, D. J., 1992. Physical Model of Source Region of Subduction Zone Volcanics. *Journal of Geophysical Research*: *Solid Earth*, 97(B2): 2037–2070. https://doi.org/10.1029/91jb02571

Defant, M. J., Drummond, M. S., 1990. Derivation of some Modern Arc Magmas by Melting of Young Subducted Lithosphere. *Nature*, 347(6294): 662–665. https://doi.org/10.1038/347662a0

Defant, M. J., Richerson, P. M., de Boer, J. Z., et al., 1991. Dacite Genesis Via both Slab Melting and Differentiation: Petrogenesis of La Yeguada Volcanic Complex, Panama. *Journal of Petrology*, 32(6): 1101–1142. https://doi.org/10.1093/petrology/32.6.1101

Eyuboglu, Y., Chung, S. L., Santosh, M., et al., 2011. Transition from Shoshonitic to Adakitic Magmatism in the Eastern Pontides, NE Turkey: Implications for Slab Window Melting. *Gondwana Research*, 19(2): 413–429. https://doi.org/10.1016/j.gr.2010.07.006

Eyuboglu, Y., Santosh, M., Yi, K., et al., 2012. Discovery of Miocene Adakitic Dacite from the Eastern Pontides Belt (NE Turkey) and a Revised Geodynamic Model for the Late Cenozoic Evolution of the Eastern Mediterranean Region. *Lithos*, 146/147: 218–232. https://doi.org/10.1016/j.lithos.2012.04.034

Ghasemi, H., Rezaei-Kahkhaei, M., 2015. Petrochemistry and Tectonic Setting of the Davarzan-Abbasabad Eocene Volcanic (DAEV) Rocks, NE Iran. *Mineralogy and Petrology*, 109(2): 235–252. https://doi.org/10.1007/s00710-014-0353-3

Gill, J. B., 1981. Orogenic Andesites and Plate Tectonics. Springer, Berlin. 390

Gorton, M. P., Schandl, E. S., 2000. From Continents to Island Arcs: A Geochemical Index of Tectonic Setting for Arc-Related and Within-Plate Felsic to Intermediate Volcanic Rocks. *The Canadian Mineralogist*, 38(5): 1065–1073. https://doi.org/10.2113/gscanmin.38.5.1065

Guest, B., Horton, B. K., Axen, G. J., et al., 2007. Middle to Late Cenozoic Basin Evolution in the Western Alborz Mountains: Implications for the Onset of Collisional Deformation in Northern Iran. *Tectonics*, 26(6): 1–26. https://doi.org/10.1029/2006tc002091

Hamilton, W. B., 1988. Plate Tectonics and Island Arcs. *Geological Society of America Bulletin*, 100(10): 1503–1527. https://doi.org/10.1130/0016-7606(1988)100<1503:ptaia>2.3.co;2

Harker, A., 1909. The Natural History of Igneous Rocks. Methuen, London. 255

Harvey, J., Baxter, E. F., 2009. An Improved Method for TIMS High Precision Neodymium Isotope Analysis of very Small Aliquots (1–10 ng). *Chemical Geology*, 258(3/4): 251–257. https://doi.org/10.1016/j.chemgeo.2008.10.024

Hassanzadeh, J., Axen, G. J., Guest, B., et al., 2004. The Alborz and NW Urumieh-Dokhtar Magmatic Belts, Iran: Rifted Parts of a Single Ancestral Arc. *Geol. Soc. Am. Abstr. Programs*, 36(5): 434

Hastie, A. R., Kerr, A. C., McDonald, I., et al., 2010. Geochronology, Geochemistry and Petrogenesis of Rhyodacite Lavas in Eastern Jamaica: A New Adakite Subgroup Analogous to Early Archaean Continental Crust?. *Chemical Geology*, 276(3/4): 344–359. https://doi.org/10.1016/j.chemgeo.2010.07.002

He, Y. S., Li, S. G., Hoefs, J., et al., 2013. Sr-Nd-Pb Isotopic Compositions of Early Cretaceous Granitoids from the Dabie Orogen: Constraints on the Recycled Lower Continental Crust. *Lithos*, 156–159: 204–217. https://doi.org/10.1016/j.lithos.2012.10.011

Hosseini, S. H., Sadeghian, M., Zhai, M. G., et al., 2015. Petrology, Geochemistry and Zircon U-Pb Dating of Band-E-Hezarchah Metabasites (NE Iran): An Evidence for Back-Arc Magmatism along the Northern Active Margin of Gondwana. *Geochemistry*, 75(2): 207–218. https://doi.org/10.1016/j.chemer.2015.02.002

Hyndman, R. D., Currie, C. A., Mazzotti, S. P., 2005. Subduction Zone Backarcs, Mobile Belts, and Orogenic Heat. *GSA Today*, 15(2): 4–10. https://doi.org/10.1130/1052-5173(2005)015<4:szbmba>2.0.co;2

Jenner, F. E., O'Neill, H. S. C., 2012. Analysis of 60 Elements in 616 Ocean Floor Basaltic Glasses. *Geochemistry*, *Geophysics*, *Geosystems*, 13(2): Q02005. https://doi.org/10.1029/2011gc004009

Kaygusuz, A., 2009. K/Ar Ages and Geochemistry of the Post-Collisional

Volcanic Rocks in the Ilica (Erzurum) Area, Eastern Turkey. *Neues Jahrbuch für Mineralogie-Abhandlungen*, 186(1): 21–36. https://doi.org/10.1127/0077-7757/2009/0134

Kaygusuz, A., Aslan, Z., Siebel, W., et al., 2011. Geochemical and Sr-Nd Isotopic Characteristics of Post-Collision Calc-Alkaline Volcanics in Eastern Pontide (NE Turkey). *Turkish Journal of Earth Sciences*, 20: 137–159

Karsli, O., Uysal, İ., Dilek, Y., et al., 2013. Geochemical Modelling of Early Eocene Adakitic Magmatism in the Eastern Pontides, NE Anatolia: Continental Crust or Subducted Oceanic Slab Origin?. *International Geology Review*, 55(16): 2083–2095. https://doi.org/10.1080/01431161.2013.819958

Keskin, M., Pearce, J. A., Kempton, P. D., et al., 2006. Magma-Crust Interactions and Magma Plumbing in a Postcollisional Setting: Geochemistry Evidence from the Erzurum Kars Volcanic Plateau, Eastern Turkey. In: Dilek, Y., Pavlides, S., eds., Postcollisional Tectonics and Magmatism in the Mediterranean Region and Asia. *Geol. Soc. Am.*, *Special Publication*, 409: 475–505

Kusky, T. M., Windley, B. F., Polat, A., 2018. Geological Evidence for the Operation of Plate Tectonics Throughout the Archean: Records from Archean Paleo-Plate Boundaries. *Journal of Earth Science*, 29(6): 1291–1303. https://doi.org/10.1007/s12583-018-0999-6

Lentz, D. R., 1998. Petrogenetic Evolution of Felsic Volcanic Sequences Associated with Phanerozoic Volcanic-Hosted Massive Sulphide Systems: The Role of Extensional Geodynamics. *Ore Geology Reviews*, 12(5): 289–327. https://doi.org/10.1016/s0169-1368(98)00005-5

Li, C. F., Li, X. H., Li, Q. L., et al., 2012a. Simultaneous Determination of ^{143}Nd/^{144}Nd and ^{147}Sm/^{144}Nd Ratios and Sm-Nd Contents from the Same Filament Loaded with Purified Sm-Nd Aliquot from Geological Samples by Isotope Dilution Thermal Ionization Mass Spectrometry. *Analytical Chemistry*, 84(14): 6040–6047. https://doi.org/10.1021/ac300786x

Li, C. F., Li, X. H., Li, Q. L., et al., 2012b. Rapid and Precise Determination of Sr and Nd Isotopic Ratios in Geological Samples from the Same Filament Loading by Thermal Ionization Mass Spectrometry Employing a Single-Step Separation Scheme. *Analytica Chimica Acta*, 727: 54–60. https://doi.org/10.1016/j.aca.2012.03.040

Li, D., He, D. F., Qi, X. F., et al., 2015. How was the Carboniferous Balkhash-West Junggar Remnant Ocean Filled and Closed? Insights from the Well Tacan-1 Strata in the Tacheng Basin, NW China. *Gondwana Research*, 27(1): 342–362. https://doi.org/10.1016/j.gr.2013.10.003

Lucci, F., Rossetti, F., White, J. C., et al., 2016. Tschermak Fractionation in Calc-Alkaline Magmas: The Eocene Sabzevar Volcanism (NE Iran). *Arabian Journal of Geosciences*, 9(10): 573. https://doi.org/10.1007/s12517-016-2598-0

Lundblad, S. P., 1994. Evolution of Small Carbonate Platforms in the Umbria-Marche Apennines, Italy: [Dissertation]. The University of North Carolina at Chapel Hill, North Carolina, USA

Ma, Q., Zheng, J. P., Xu, Y. G., et al., 2015. Are Continental "Adakites" Derived from Thickened or Foundered Lower Crust?. *Earth and Planetary Science Letters*, 419: 125–133. https://doi.org/10.1016/j.epsl.2015.02.036

McQuarrie, N., Stock, J. M., Verdel, C., et al., 2003. Cenozoic Evolution of Neotethys and Implications for the Causes of Plate Motions. *Geophysical Research Letters*, 30(20): 2036. https://doi.org/10.1029/2003gl017992

Martin, H., Smithies, R. H., Rapp, R., et al., 2005. An Overview of Adakite, Tonalite-Trondhjemite-Granodiorite (TTG), and Sanukitoid: Relationships and some Implications for Crustal Evolution. *Lithos*, 79(1/2): 1–24. https://doi.org/10.1016/j.lithos.2004.04.048

Martin, H., 1994. The Archean Grey Gneisses and the Genesis of the Conti-

nental Crust. In: Condie, K. C., ed., Archean Crustal Evolution. Elsevier, Amsterdam. 205–259

Mathieu, L., Racicot, D., 2019. Petrogenetic Study of the Multiphase Chibougamau Pluton: Archaean Magmas Associated with Cu-Au Magmato-Hydrothermal Systems. *Minerals*, 9(3): 174. https://doi.org/10.3390/min9030174

Mehdipour Ghazi, J., Moazzen, M., 2015. Geodynamic Evolution of the Sanandaj-Sirjan Zone, Zagros Orogen, Iran. *Turkish Journal of Earth Sciences*, 24: 513–528. https://doi.org/10.3906/yer-1404-12

Middlemost, E. A. K., 1986. Magmas and Magmatic Rocks: An Introduction to Igneous Petrology. Addison-Wesley Longman. 280

Moghadam, H. S., Rossetti, F., Lucci, F., et al., 2016. The Calc-Alkaline and Adakitic Volcanism of the Sabzevar Structural Zone (NE Iran): Implications for the Eocene Magmatic Flare-up in Central Iran. *Lithos*, 248–251: 517–535. https://doi.org/10.1016/j.lithos.2016.01.019

Mohajjel, M., Fergusson, C. L., Sahandi, M. R., 2003. Cretaceous–Tertiary Convergence and Continental Collision, Sanandaj-Sirjan Zone, Western Iran. *Journal of Asian Earth Sciences*, 21(4): 397–412. https://doi.org/10.1016/s1367-9120(02)00035-4

Mori, L., Gómez-Tuena, A., Cai, Y., et al., 2007. Effects of Prolonged Flat Subduction on the Miocene Magmatic Record of the Central Trans-Mexican Volcanic Belt. *Chemical Geology*, 244(3/4): 452–473. https://doi.org/10.1016/j.chemgeo.2007.07.002

Moyen, J. F., Martin, H., 2012. Forty Years of TTG Research. *Lithos*, 148: 312–336. https://doi.org/10.1016/j.lithos.2012.06.010

Moyen, J. F., 2009. High Sr/Y and La/Yb Ratios: The Meaning of the "Adakitic Signature". *Lithos*, 112(3/4): 556–574. https://doi.org/10.1016/j.lithos.2009.04.001

Murphy, J. B., 2007. Arc-Magmatism II: Geochemical and Isotopic Characteristics. *Geoscience Canada*, 34: 7–35

Nakamura, N., 1974. Determination of REE, Ba, Fe, Mg, Na and K in Carbonaceous and Ordinary Chondrites. *Geochimica et Cosmochimica Acta*, 38(5): 757–775. https://doi.org/10.1016/0016-7037(74)90149-5

Nezafati, N., 2015. Mineral Resources of Iran: An Overview. In: 66th Bergund Hüttenmännischer Tag (BHT). June 17–19, 2015, Freiberg, Germany. 1–33

Nicholson, K. N., Black, P. M., Hoskin, P. W. O., et al., 2004. Silicic Volcanism and Back-Arc Extension Related to Migration of the Late Cainozoic Australian-Pacific Plate Boundary. *Journal of Volcanology and Geothermal Research*, 131(3/4): 295–306. https://doi.org/10.1016/s0377-0273(03)00382-2

Özyurt, M., Altunkaynak, Ş., 2020. Origin of Eocene Adakitic Magmatism in Northwest Turkey. *Journal of Asian Earth Sciences*, 190: 104147. https://doi.org/10.1016/j.jseaes.2019.104147

Pearce, J. A., 2014. Immobile Element Fingerprinting of Ophiolites. *Elements*, 10(2): 101–108. https://doi.org/10.2113/gselements.10.2.101

Pearce, J. A., Harris, N. B. W., Tindle, A. G., 1984. Trace Element Discrimination Diagrams for the Tectonic Interpretation of Granitic Rocks. *Journal of Petrology*, 25(4): 956–983. https://doi.org/10.1093/petrology/25.4.956

Pearce, J. A., Peate, D. W., 1995. Tectonic Implications of the Composition of Volcanic ARC Magmas. *Annual Review of Earth and Planetary Sciences*, 23(1): 251–285. https://doi.org/10.1146/annurev.ea.23.050195.001343

Peccerillo, A., Taylor, S. R., 1976. Geochemistry of Eocene Calc-Alkaline Volcanic Rocks from the Kastamonu Area, Northern Turkey. *Contributions to Mineralogy and Petrology*, 58(1): 63–81. https://doi.org/10.1007/bf00384745

Peterman, Z. E., Barker, F., 1976. Rb-Sr Whole-Rock Age of Trondhjemites and Related Rocks of the South Western Trondheim Region, Norway. *United States Geological Survey Open File Report*, 76: 1–17

Pirajno, F., 2016. A Classification of Mineral Systems, Overviews of Plate Tectonic Margins and Examples of Ore Deposits Associated with Convergent Margins.

Gondwana Research, 33: 44–62. https://doi.org/10.1016/j.gr.2015.08.013

Plank, T., 2014. The Chemical Composition of Subducting Sediments. In: Keeling, R. F., ed., Treatise on Geochemistry. Elsevier, Amsterdam. 607–629. https://doi.org/10.1016/b978-0-08-095975-7.00319-3

Rapp, R. P., Watson, E. B., 1995. Dehydration Melting of Metabasalt at 8–32 kbar: Implications for Continental Growth and Crust-Mantle Recycling. *Journal of Petrology*, 36(4): 891–931. https://doi.org/10.1093/petrology/36.4.891

Ricou, L. E., Braud, J., Brunn, J. H., 1977. Le Zagros. *Mémoire hors Série de la Société Géologique de France*, 8: 33–52

Rollinson, H., 1993. Using Geochemical Data: Evaluation, Presentation, Interpretation. Routledge, New York. 352

Rudnick, R. L., Gao, S., 2003. Composition of the Continental Crust. In: Holland, H. D., Turekian, K. K., eds., Treatise Geochem. 3, Elsevier, Oxford. 1–64

Sheth, H. C., Torres-Alvarado, I. S., Verma, S. P., 2002. What is the "Calc-Alkaline Rock Series"?. *International Geology Review*, 44(8): 686–701. https://doi.org/10.2747/0020-6814.44.8.686

Stampfli, G. M., Borel, G. D., 2002. A Plate Tectonic Model for the Paleozoic and Mesozoic Constrained by Dynamic Plate Boundaries and Restored Synthetic Oceanic Isochrons. *Earth and Planetary Science Letters*, 196(1/2): 17–33. https://doi.org/10.1016/s0012-821x(01)00588-x

Sun, S. S., McDonough, W. F., 1989. Chemical and Isotopic Systematics of Oceanic Basalts: Implications for Mantle Composition and Processes. *Geological Society, London, Special Publications*, 42(1): 313–345. https://doi.org/10.1144/gsl.sp.1989.042.01.19

Temel, A., Gündoğdu, M. N., Gourgaud, A., 1998. Petrological and Geochemical Characteristics of Cenozoic High-K Calc-Alkaline Volcanism in Konya, Central Anatolia, Turkey. *Journal of Volcanology and Geothermal Research*, 85(1/2/3/4): 327–354. https://doi.org/10.1016/s0377-0273(98)00062-6

Temizel, İ., Arslan, M., Ruffet, G., et al., 2012. Petrochemistry, Geochronology and Sr-Nd Isotopic Systematics of the Tertiary Collisional and Post-Collisional Volcanic Rocks from the Ulubey (Ordu) Area, Eastern Pontide, NE Turkey: Implications for Extension-Related Origin and Mantle Source Characteristics. *Lithos*, 128–131: 126–147. https://doi.org/10.1016/j.lithos.2011.10.006

Verdel, C., Wernicke, B. P., Hassanzadeh, J., et al., 2011. A Paleogene Extensional Arc Flare-up in Iran. *Tectonics*, 30(3): TC3008. https://doi.org/10.1029/2010tc002809

Wang, Z. H., Zhao, Y., Zou, H. B., et al., 2007. Petrogenesis of the Early Jurassic Nandaling Flood Basalts in the Yanshan Belt, North China Craton: A Correlation between Magmatic Underplating and Lithospheric Thinning. *Lithos*, 96(3/4): 543–566. https://doi.org/10.1016/j.lithos.2006.12.004

Wang, Q., Wyman, D. A., Xu, J. F., et al., 2008. Triassic Nb-Enriched Basalts, Magnesian Andesites, and Adakites of the Qiangtang Terrane (Central Tibet): Evidence for Metasomatism by Slab-Derived Melts in the Mantle Wedge. *Contributions to Mineralogy and Petrology*, 155(4): 473–490. https://doi.org/10.1007/s00410-007-0253-1

Wallace, G. S., Bergantz, G. W., 2002. Wavelet-Based Correlation (WBC) of Zoned Crystal Populations and Magma Mixing. *Earth and Planetary Science Letters*, 202(1): 133–145. https://doi.org/10.1016/s0012-821x(02)00762-8

Wedepohl, K. H., 1995. The Composition of the Continental Crust. *Geochimica et Cosmochimica Acta*, 59(7): 1217–1232. https://doi.org/10.1016/0016-7037(95)00038-2

Whalen, J. B., Currie, K. L., Chappell, B. W., 1987. A-Type Granites: Geochemical Characteristics, Discrimination and Petrogenesis. *Contributions to Mineralogy and Petrology*, 95(4): 407–419. https://doi.org/10.1007/bf00402202

Whitney, D. L., Evans, B. W., 2010. Abbreviations for Names of Rock-Forming Minerals. *American Mineralogist*, 95(1): 185–187. https://doi.org/10.2138/am.2010.3371

Winchester, J. A., Floyd, P. A., 1977. Geochemical Discrimination of Different Magma Series and Their Differentiation Products Using Immobile Elements. *Chemical Geology*, 20: 325–343. https://doi.org/10.1016/0009-2541(77)90057-2

Wood, D. A., Joron, J. L., Treuil, M., 1979. A Re-Appraisal of the Use of Trace Elements to Classify and Discriminate between Magma Series Erupted in Different Tectonic Settings. *Earth and Planetary Science Letters*, 45(2): 326–336. https://doi.org/10.1016/0012-821x(79)90133-x

Xu, J. F., Shinjo, R., Defant, M. J., et al., 2002. Origin of Mesozoic Adakitic Intrusive Rocks in the Ningzhen Area of East China: Partial Melting of Delaminated Lower Continental Crust?. *Geology*, 30(12): 1111–1114. https://doi.org/10.1130/0091-7613(2002)030<1111:oomair>2.0.co;2

Yousefi, F., 2017. Petrogenesis and Isotope Geology of Post Eocene Intrusive Rocks of Torud-Ahmad Abad Magmatic Belt (SE of Shahrood): [Dissertation]. Shahrood University of Technology, Shahrood. 247 (in Persian with English Abstract)

Yousefi, F., Sadeghian, M., Wanhainen, C., et al., 2017a. Geochemistry, Petrogenesis and Tectonic Setting of Middle Eocene Hypabyssal Rocks of the Torud-Ahmad Abad Magmatic Belt: An Implication for Evolution of the Northern Branch of Neo-Tethys Ocean in Iran. *Journal of Geochemical Exploration*, 178: 1–15. https://doi.org/10.1016/j.gexplo.2017.03.008

Yousefi, F., Sadeghian, M., Wanhainen, C., et al., 2017b. Mineral Chemistry and *P-T* Conditions of the Adakitic Rocks from Torud-Ahmad Abad Magmatic Belt, S-SE Shahrood, NE Iran. *Journal of Geochemical Exploration*, 182: 110–120. https://doi.org/10.1016/j.gexplo.2017.09.006

Yumul, G. P. Jr., Brown, W. W., Dimalanta, C. B., et al., 2017. Adakitic Rocks in the Masara Gold-Silver Mine, Compostela Valley, Mindanao, Philippines: Different Places, Varying Mechanisms?. *Journal of Asian Earth Sciences*, 142: 45–55. https://doi.org/10.1016/j.jseaes.2016.06.005

Zhang, X. R., Zhao, G. C., Eizenhöfer, P. R., et al., 2016. Tectonic Transition from Late Carboniferous Subduction to Early Permian Post-Collisional Extension in the Eastern Tianshan, NW China: Insights from Geochronology and Geochemistry of Mafic-Intermediate Intrusions. *Lithos*, 256/257: 269–281. https://doi.org/10.1016/j.lithos.2016.04.006

Zheng, Y. F., 2019. Subduction Zone Geochemistry. *Geoscience Frontiers*, 10(4): 1223–1254. https://doi.org/10.1016/j.gsf.2019.02.003

Zhu, D. C., Zhao, Z. D., Pan, G. T., et al., 2009. Early Cretaceous Subduction-Related Adakite-Like Rocks of the Gangdese Belt, Southern Tibet: Products of Slab Melting and Subsequent Melt-Peridotite Interaction?. *Journal of Asian Earth Sciences*, 34(3): 298–309. https://doi.org/10.1016/j.jseaes.2008.05.003

Zindler, A., Hart, S., 1986. Chemical Geodynamics. *Annual Review of Earth and Planetary Sciences*, 14(1): 493–571. https://doi.org/10.1146/annurev.ea.14.050186.002425